REVIEW

Check for updates

Recent developments in conducting polymers: applications for electrochemistry

Somayeh Tajik,[a] Hadi Beitollahi, [ID] *[b] Fariba Garkani Nejad,[c] Iran Sheikh Shoaie,[c] Mohammad A. Khalilzadeh, [ID] [d] Mehdi Shahedi Asl,[e] Quyet Van Le [ID] *[f] Kaiqiang Zhang,[g] Ho Won Jang [ID] *[g] and Mohammadreza Shokouhimehr [ID] *[g]

Scientists have categorized conductive polymers as materials having strongly reversible redox behavior and uncommon combined features of plastics and metal. Because of their multifunctional characteristics, *e.g.*, simplistic synthesis, acceptable environmental stability, beneficial optical, electronic, and mechanical features, researchers have largely considered them for diverse applications. Therefore, their capability of catalyzing several electrode reactions has been introduced as one of their significant features. A thin layer of the conducting polymer deposited on the substrate electrode surface can augment the electrode process kinetics of several solution species. Such electrocatalytic procedures with modified conducting polymer electrodes can create beneficial utilization in diverse fields of applied electrochemistry. This review article explores typical recent applications of conductive polymers (2016–2020) as active electrode materials for energy storage applications, electrochemical sensing, and conversion fields such as electrochemical supercapacitors, lithium-ion batteries, fuel cells, and solar cells.

1. Introduction

It is well known that electrochemistry entails phenomena in which a chemical modification results from electric forces and, conversely, chemical processes generate electric forces. This field involves features and behaviors of the electrolytic conductors in solid or liquid form. Numerous such phenomena occur at the electrolytic and electronic conductor interface, wherein the electric charge passage is connected to a redox chemical reaction. This reaction rate may be followed as an electric current with increased sensitivity. The contacts make up the electrodes of galvanic cells that may be utilized to convert chemicals to electrical energy as batteries or generate chemical products *via* electrolysis.[1,2]

[a]*Research Center for Tropical and Infectious Diseases, Kerman University of Medical Sciences, Kerman, Iran*

[b]*Environment Department, Institute of Science and High Technology and Environmental Sciences, Graduate University of Advanced Technology, Kerman, Iran. E-mail: h.beitollahi@yahoo.com*

[c]*Department of Chemistry, Faculty of Science, Shahid Bahonar University of Kerman, Kerman 76175-133, Iran*

[d]*Department of Biomaterials, College of Natural Resources, North Carolina State University, Raleigh, USA*

[e]*Marine Additive Manufacturing Centre of Excellence (MAMCE), University of New Brunswick, Fredericton, NB, E3B 5A1, Canada*

[f]*Institute of Research and Development, Duy Tan University, Da Nang 550000, Vietnam. E-mail: levanquyet@dtu.edu.vn*

[g]*Department of Materials Science and Engineering, Research Institute of Advanced Materials, Seoul National University, Seoul 08826, Republic of Korea. E-mail: mrsh2@snu.ac.kr; hwjang@snu.ac.kr*

The development of novel techniques for performing fast *in situ* analyses has been considered as a major challenge as they present high sensitivity and accuracy for the detection of diverse materials with various features in real samples. Experts in the field have demonstrated that electroanalytical procedures would be among the encouraging alternatives for the quantitative and qualitative analyses of replacing the traditional techniques. Electrochemical sensing mechanisms are accompanied by benefits like simplistic instruments, miniaturization, higher selectivity and sensitivity, simplified utilization, minor sample pretreatment, portability, and shorter analysis time.[3–5] Put differently, electrodes are capable of sensing substances found in the host with no damages to the host system. Nonetheless, electrochemical sensors suffer from limitations such as the electrochemically active interference in the sample, poor stability, difficult electron transfer pathway, as well as decreased limits of detection (LOD) and sensitivity.[6,7] Consequently, diverse electrochemical procedures are combined with various sensing electrodes to augment their LOD and sensitivity *via* the modification of the electrode materials.

The storage and conversion of energies contribute significantly to the conservation of the available energy and improvement of its usage because of the existence of multiple energy resources in nature. Notably, a shorter storage time of just a few hours would be crucial in majority of applications; nonetheless, a lengthier storage of few months is sometimes necessary. In this aspect, electrochemical energy storage (EES) technology has been introduced as an encouraging tool for the storage of electricity in small- and large-scale applications due

to the flexibility, higher energy conversion efficiency, as well as easy maintenance.[8,9]

It is worth noting that the use of instruments for electrochemical energy storage and conversion enable the storage of surplus energy in the case of a greater electricity supply than demand, and its release in the case of a greater demand than supply. Such a situation leads to higher efficiency of the grid, higher reliability, as well as lower costs. On the one hand, the grid-scale energy storage needs electrochemical machines with suitable power and energy output features, longer cycle life, higher efficiency, and lower costs. Therefore, accelerated advancements in devising electroactive substances for EES tools offered numerous attractive organic mechanisms that are appropriate for higher power and energy uses.[10–12]

On the other hand, researchers have been greatly attracted by organic π-conjugated polymers since Lethebyin showed the electrochemical procurement and description of polyaniline (PANI) created by oxidizing aniline on a platinum electrode in dilute sulfuric acid for the first time.[13] As such, the conductivity of polyacetylene has been examined and increased ten-fold by using iodine vapors. Polyacetylene instability in air has resulted in the discovery of diverse, novel conducting polymers (CPs) to be utilized in basic studies and industrial applications.[14–16] Therefore, since Heeger, MacDiarmid, and Shirakawa were jointly granted the Nobel Prize in Chemistry in 2000 for their leading research on CPs, academic and industrial researchers have given significant consideration to these materials. Earlier studies on these materials have been about the true mechanism of polypyrrole (PPy) formation. Park's group intensively investigated CPs electrochemistry and showed the autocatalytic growth system of PANI with its growth kinetics on the surface of the electrode.[17–21]

Generally, CPs have been introduced as one of the classes of organic polymers with metallic or semiconductor features, such as magnetic, electrical, optical, and electronic properties, to retain the characteristics of the conventional organic polymers, including simpler synthesis, corrosion resistance, and lower costs. These materials may be either insulators or semiconductors in the neutral or undoped form, which may be converted to the doped form through the redox reaction to form delocalized charge carriers. However, an advantage of the CPs in comparison to numerous organic polymers has been their adjustable chemical structures that may be modified to alter the conductivity of the polymer. The CPs have charge mobility along with their p-electron backbones that handle their uncommon electronic features such as lower energy optical transition, better electrical conductivity, higher surface area, high electron affinity, and mechanical flexibility.[22–28] The most effective parameters constructing the physical properties of CPs are conjugation length, degree of crystallinity, and intra- and inter-chain interactions.

One of the applicable methods for preparing CPs is the anodic oxidation of the appropriate monomers, *e.g.*, thiophene, aniline, *etc.* From the viewpoint of molecular electrochemistry, the most relevant aspects for clarifying the mechanism of electropolymerization are the formation of oligomers, nucleation and growth steps, and the formation of the polymeric

materials. Mechanistic details are important for optimizing the conditions of electropolymerization. They play important roles in determining the quality of the produced CPs. A central point of electrochemical research is the analysis of the "doping" process. Even in the earliest stages of research on CPs, there was no doubt that these processes were not comparable with the classic doping of inorganic semiconductors. They correspond to oxidation in the case of p-doping or reduction in the case of n-doping. Using the electrochemical terminology, this means that the doping process corresponds to redox reactions in the polymer matrix. It is very important to know the phenomenological details of such redox reactions, in which potential range charging occurs at the maximum level of oxidation before material degradation.[29–31]

On the other hand, the experts in the field have been considerably attracted by the CPs because of the respective potent applications in energy storage and conversion, electrochemical sensors, and so on. Therefore, this review deals with the new studies of the CPs as (i) electrodes for electrochemical sensors and (ii) electrochemical energy storage and conversion tools like the electrode substances for super-capacitors, fuel cells, lithium-ion batteries (LIBs), and solar cells.

2. Electrochemical features of the conducting polymers

In 1977, the organic polymer polyacetylene was discovered, which when doped with iodine exhibited a unique, high electronic conductivity for organic material. Since then, researchers have investigated conducting polymers because of their specific electrical features.[16] Despite traditional organic polymers, these materials enjoy certain features like electrical conductivity, higher electron affinity, as well as redox activities.[32]

These materials include the π-electron backbone controlling uncommon electronic features like the electrical conductivity, lower energy optical transition, higher electron affinity as well as lower ionization potential. Moreover, such an extended π-conjugated system of the conducting polymer possesses alternating single- and double-bonds in line with the polymer chain.[33,34]

It is worth mentioning that the conduction mechanism in these types of polymers is highly complicated because they exhibit conductivity through a range of approximately 15 orders of magnitude, and several of them contain diverse mechanisms in distinct regimes. Conducting polymers have shown greater electrical conductivity *via* multiple orders of magnitude. Moreover, CPs may be doped electrochemically, implying that CPs oxidation creates a p-doped state and CPs reduction leads to an n-doped state. Redox reactions may control the conductivity of CPs. Electrochemical preparation techniques may address the features, morphology, thickness, and conductivity of the polymer. In general, researchers have applied the terms soliton, polaron, and bipolar for explaining the electronic phenomena in such systems.[35,36] The conductivity in the conducting polymers is affected by diverse parameters like the conjugation length, polaron length, overall length of the chain, as well as

charge transfer to the near-by molecules.[37] Such conditions could be justified by several models based on inter-soliton hopping, hopping between the localized state assisted by the lattice vibrations, intra-chain hopping of the bi-polarons, varied range hopping in 3 sizes, as well as the charging energy restricting the tunneling between the conducting domains.[38]

It is possible to functionalize CPs and monomers with distinctive materials for tailoring their features. Therefore, adding the substituents ameliorates the performance and physicochemical features of the major polymer chain such as the enhanced mechanical and electrical characteristics. For improving CPs features, it is possible to prepare the CPs composite from the strongly conductive nanomaterials, as well as catalysts.[36]

3. Chemical structure of CPs

The electronic properties of CPs differ from the inorganic crystalline semiconductors in two major areas; *i.e.*, long-range order and their molecular nature. For a polymer to become conducting, it must contain overlapping π-molecular orbitals and a high degree of π-bond conjugation. This comprehensive π-conjugated system of the CPs has irregular single and double bonds all along the polymer chain (Fig. 1). When a highly conjugated polymer is in its neutral state, it is essentially an insulating material. It is only upon removal of a π-bond electron from the conjugated polymer backbone to form a radial cation defect (called a polaron) that the insulating polymer becomes conductive. Removal of π-bond electrons causes the remaining electrons in the π-orbitals to become delocalized along the length of the conjugated polymer backbone, thereby enabling the free movement of the polymer along the chain. The formation of the positively charged polymer backbone is accompanied by the incorporation of a dopant anion, which has the effect of electrostatically balancing the positive charges.[39,40]

Some typical CPs include PPY, PANI, polycarbazole (PCZ), polythiophene (PTh) and its derivatives of poly(3,4-ethylene dioxythiophene) (PEDOT), and poly(3-hexylthiophene) (P3HT). These polymers contain the sp^2 structure, which transports charge carriers (Fig. 2a). CPs have advantages such as controllable chemical/electrochemical properties and adjustable electrical conductivities from 10^{-11} to 10^5 S cm^{-1} upon doping

(Fig. 2b). They are soft and extendable, similar to conventional polymers.[41,42]

The chemical structure of PPy consists of repeating units of the pyrrole monomer (a nitrogen-containing aromatic ring). The mechanism of pyrrole polymerization most likely involves oxidation, deprotonation, and crosslinking. The doping process of PPy is p-doping, where the polymer is oxidized and has a positive charge. One of the two leading theories is that pyrrole monomers are first oxidized to release a radical cation, followed by the coupling of two cations and the production of a bipyrrole. As oxidation continues, the chain continues to grow. The second theory advocates that a cation reacts with a neutral monomer. After oxidation and deprotonation, a dimer is formed, and the polymer chains keep growing by repeating this process. Eventually, a conduction band is developed by the delocalized electrons from the double bond in the backbone of PPy. PPy exhibits good electrical conductivity under physiological conditions due to its p-type conduction.[43,44]

PANI chains, resulting from the oxidative polymerization of aniline, are composed of two structural units, namely, the reduced [B–NH–B–NH], and the oxidized [B–N=Q=N⁻] repeat units, where B denotes the benzenoid and Q denotes a quinoid ring. The quinoid ring and benzenoid can transform into each other *via* the redox process. The protonated PANI chain is electrically conductive only when $x : y = 1 : 1$ (*i.e.*, benzenoid : quinoid = 3 : 1). PANI has a reversible acid/base doping process. PANI is conductive in acid form, while it is insulating in the emeraldine base form. The electrical conductivity of PANI increases with doping from the undoped insulating emeraldine base form ($\sigma < 10^{-10}$ mho cm^{-1}) to the fully doped, conducting emeraldine salt form ($\sigma > 1$ mho cm^{-1}) by modulating its oxidative state through changing counter ions (dopant) and the degree of doping.[45]

Carbazole is reported to form a conducting polymer with a conductivity of 0.1–1 S cm^{-1}. It can be considered either as a derivative of pyrrole or aniline. PCZ has a bulky side chain of 4-[tris-(4-octyloxyphenyl)methyl]phenyl. Its big side chain prevents the π-stacking of polymers and reduces the interactions between polymers, which contributes to the high fluorescence efficiency, and also benefits the diffusion of explosives. Furthermore, the side chain moiety endows the polymer with good solubility and helps to form films with high quality by spin coating.[46,47]

Thiophene is an electron-rich aromatic ring, which can be oxidized to form p-doped highly conducting PThs. The electrochemical oxidation can result in well-adhering polymeric film formation. Moreover, the thickness of the polymer films can be controlled by changing the polymerization time during the electropolymerization process.[48]

PEDOT is a p-conjugated polymer that has received considerable interest due to its potential for a variety of applications. The rigid and linear conformation of PEDOT facilitates charge transport and favors its crystallization, resulting in favorable properties such as high charge/discharge capacities, fast response times, and high sensing capabilities. PEDOT is polymerized by either appropriate oxidants (chemically), or electrochemical current.[49]

Fig. 1 The π-conjugated system of conducting polymers.

Fig. 2 (a) Chemical structures of several CPs. (b) Electrical conductivity range of CPs. Reproduced with permission from ref. 42. Copyright 2020 Elsevier.

The P3HT structure involves 2D sheets of π-stacked poly(-thiophene) backbones separated by layers of *n*-hexyl side chains. It is thought that the conformation and packing of the polymer backbone plays a dominant role in the determination of its transport properties.[50]

4. Uses of the conducting polymers

4.1. Electrochemical sensing

According to the studies, electrochemical sensors and biosensors have been considered as electrochemical cells containing 3 or 2 electrodes. A characteristic 3-electrode system contains a reference, counter, and working electrode; the working electrode has a chemically stable solid conductive substance like gold, carbon, and platinum, the reference electrode generally contains the silver metal coated with a layer of silver chloride (Ag/AgCl), and a platinum wire is usually employed as an auxiliary electrode. On the contrary, a two-electrode system contains just the reference and working electrodes. Hence, it is possible to classify the electrochemical procedures into three key categories concerning the kinds of measurement, as follows:[51–53] (i) current (voltammetric & amperometric), (ii) potential difference (potentiometry), and (iii) impedance (electrochemical impedance spectroscopy), out of which the biosensors based on the current measurements have a widespread application. On the one hand, the current measurement-based sensors have been described *via* the use of the potential to a working electrode against a reference electrode and the measurement of the current. This electric current results from the electrolysis because of the electrochemical oxidation or reduction at the working electrode surface. Nevertheless, this procedure is dependent on the mass transport rate of the molecules to the electrode, as well as the rate of electron transfer at the electrode surface.[54,55]

It is notable that while developing the electroanalytical sensing mechanisms to determine different analytes, these sensing electrodes have been frequently modified with suitable substances for achieving the intended increase in the selectivity and sensitivity.[56–59] Most electrocatalytic materials are based on noble or transition metal elements, either as pure electronic conducting metals or alloys, or as electronic semiconductors. Therefore, the substitution of precious metals with inexpensive organic compounds has been the subject of many active research efforts. For example, well-defined 2D covalent organic polymers and carbon organic frameworks act similar to CPs as they also include π-conjugated polymeric layers containing heterocycles and aromatic moieties with precisely controlled molecular structures. CPs can have intrinsic electrocatalytic properties toward certain redox reactions. It is also possible to use the inter-chain cavities in these materials to incorporate metals so that electrocatalysts can be generated. CPs have also been used to immobilize redox mediators, thus boosting the homogeneous electron transfer in the catalytic cycle. This

approach is based on the efficient immobilization of biomolecules like proteins and enzymes through the very strong interactions with avidin *via* an affinity coupling with biotin. Therefore, their high conductivity and other properties discussed earlier make them suitable as catalysts for diverse redox reactions.[60–62] According to the analyses, designing and constructing the CPs-modified electrodes is highly efficient in the electrochemical sensor technology.

4.1.1. Drug analysis. One of the voltammetric sensors for the trace analyses of streptomycin (STR) was characterized in 2017. This sensor was made by the application of a glassy carbon electrode (GCE) modified with the STR-imprinted poly(pyrrole-3-carboxy acid) (PPy3C) film on electrochemically reduced graphene oxide (ERGO). The ERGO was initially deposited on the GCE surface through electroreduction and deposition of a film of the STR-imprinted PPy3C. Then, differential pulse voltammetry (DPV), scanning electron microscopy (SEM), and cyclic voltammetry (CV) were used to characterize the sensor features and morphology. Based on the optimal conditions, the sensor for STR displayed 2 linear ranges from 2–80 and 80–1000 nM concentration ranges. It also included the

LOD of 0.5 nM, reliable practicability, and acceptable molecular recognition.[63]

In their research, Dechtrirat *et al.* procured a molecularly imprinted polymer (MIP) and a nanocomposite from the gold NPs (Au NP), and poly(3,4-ethylenedioxythiophene)/poly(styrene sulfonate) (PEDOT:PSS) was deposited on a screen-printed carbon electrode (SPCE). Fig. 3 presents the procedure for the construction of the electrochemical MIP sensor to detect nitrofurantoin (NFT). The one-pot concurrent *in situ* formation of the AuNPs and PEDOT:PSS was used to prepare the nanocomposite and inkjet-coat it on the SPCE. Then, this MIP film was coated on the modified SPCE using the co-electrodeposition of *o*-phenylenediamine and resorcinol in the presence of antibiotic NFT. Researchers also used DPV and showed the linearity of the potential of nearly 0.1 V *versus* Ag/AgCl in the 1 to 1000 nM NFT concentration range with 0.1 nM LOD at S/N = 3. Such a condition was 2 orders of magnitude less than that of the control MIP sensor with any nano-composite inter-layer, which reflected the advantageous impact of AuNP-PEDOT:PSS. Analyses showed the higher reproducibility of the electrode (relative standard deviation (RSD) of 3.1% for n = 6) and selectivity in comparison to the structurally associated molecules.
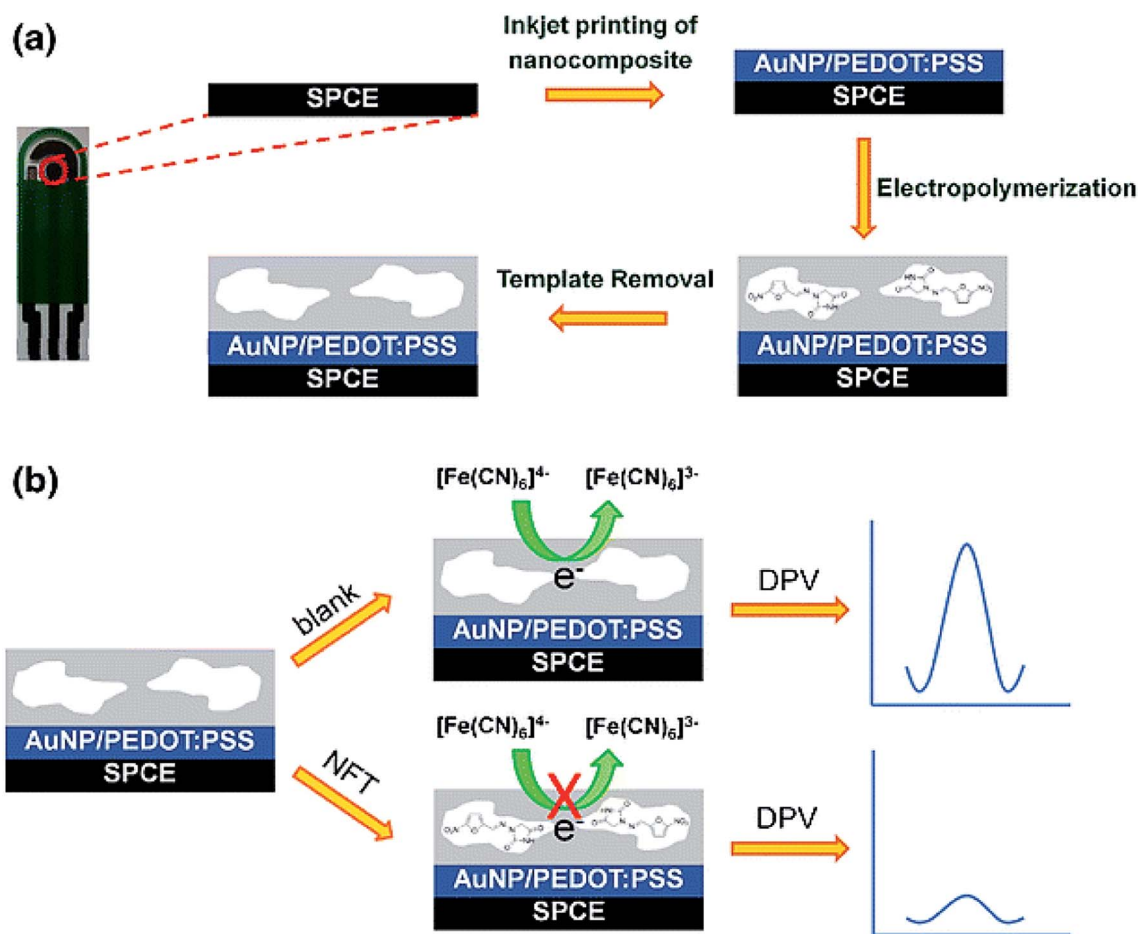

Fig. 3   The electrochemical MIP sensor for NFT determination: (a) the preparation of the electro-synthesized MIP on the nanocomposite modified SPCE. (b) Indirect voltammetric detection of NFT utilizing the $K_3[Fe(CN)_6]/K_4[Fe(CN)_6]$ as the electrochemical probe. Reproduced with permission from ref. 64. Copyright 2018 Springer.

Furthermore, it is possible to reuse it for at least 10 times, with stability for at least 45 days. Finally, researchers experienced its successful utilization for determining NFT in the (spiked) feed matrix with acceptable recovery.[64]

Furthermore, the new sensitive electrochemical technique devised by Raj *et al.* has been used for simultaneously determining dopamine (DA) and 5-hydroxy-tryptamine (5-HT) with a graphene (GR) and poly4-amino-3-hydroxy-1-naphthalene-sulfonic acid-modified screen-printed carbon sensor. The researchers applied square wave voltammetry (SWV) and CV to study the electrochemical measurements, while EIS and field emission SEM were utilized for the characterization of the surface morphology of the modified sensor. It was found that this sensor simplified DA and 5-HT analysis in a concentration range between 0.05 and 100 μM and 0.05 to 150 μM with 2 nM and 3 nM LOD, respectively. It was further examined to determine 5-HT in the plasma specimens and confirm its selectivity toward 5-HT and DA in the presence of the usual metabolites in biological fluids. Consequently, Raj *et al.* substantially confirmed the analytical usability of this new sensor for simultaneously detecting 5-HT and DA in drug formulations, blood samples, and human urine.[65]

Another study conducted by Govindasamy *et al.* addressed the design and fabrication of an affordable modified electrode based on the sensitive detection of ascorbic acid (AA) by PANI and Ni (PANI–Ni) composites. They employed EIS, energy-dispersive X-ray spectroscopy, and electrochemical techniques for characterizing the composite formation. The PANI–Ni composite was utilized for modifying SPCE and then the final modified electrode was applied in the development of the AA sensor. This modified electrode showed very good electro-catalytic activities for oxidizing AA. In the next stage,

researchers designed an amperometric sensor with the PANI–Ni composite that exhibited sensitive prompt signals for AA. Analyses showed a 2–1210 μM linear range, 0.4 μM LOD, and 0.479 μA μM cm^{-2} sensitivities; the researchers approved the acceptable reproducibility, stability, and iterability of their electrode. Finally, they confirmed the functional usability of the electrode in the samples of human urine.[66]

Talib *et al.* investigated the development of an electrochemical immuno-sensor based on poly(3,4-ethylene-dioxythiophene)/graphene oxide (PEDOT/GO)-modified SPCE to detect clenbuterol (CLB) (Fig. 4). Electropolymerization was used to modify the SPCE with the PEDOT/GO as a sensor platform, whereas electrochemical assay was implemented with the direct competitive format wherein free CLB and clenbuterol-horseradish peroxidase (CLB-HRP) in the solution would have competition for forming the binding with polyclonal anti-clenbuterol antibody (Ab) immobilized on the surface of the modified electrode. Researchers observed a linear standard CLB calibration curve with R^2 of 0.9619 and 0.196 ng mL^{-1} LOD. They analyzed the milk sample and showed the ability of their immunosensor to detect CLB in real samples. Notably, their outputs could be compared with the enzyme-immunosorbent assay (ELISA).[67]

The investigation conducted by Sağlam *et al.* provided a new molecularly imprinted (MI) electrochemical sensor for selectively determining DA in the presence of an 80-fold excess of AA and UA. They used the Au NPs (Aunano)-decorated GCE coated with the poly(carbazole (Cz)-*co*-aniline (ANI)) copolymer film, incorporating DA as the template (DA imprinted-GC/P(Cz-*co*-ANI)-Aunano electrode, *i.e.*, the DA-MIP-Aunano electrode. In the DA determination, the sensor electrode exhibited greater electroactivity for the analyte oxidation in 0.2 M phosphate
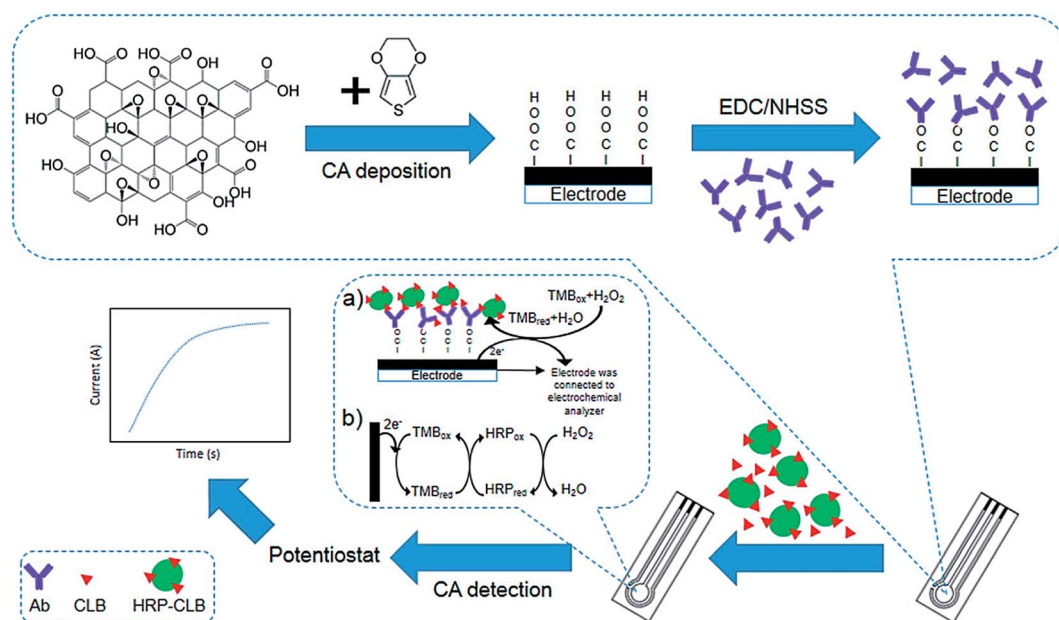

Fig. 4 Construction of the clenbuterol hydrochloride (CLB) immunosensor. (a) The electrochemical immunosensor format was utilized to detect CLB. (b) The indirect electron transfer for the TMB redox is displayed by the complex TMB/HRP/H$_2$O$_2$ enzyme reaction on the modified SPCE to reduce the creation of the current. Reproduced with permission from ref. 67. Copyright 2018 MDPI.

buffer (PB) at pH 7. SWV was run into 10^{-4} to 10^{-5} M of DA and the oxidation peak potential was seen at 0.16 V. The limit of quantification (LOQ) and LOD were 6.7×10^{-6} M and 2.0×10^{-6} M, respectively. Furthermore, the binary and ternary synthetic mixtures, DA–AA, DA–UA–AA, and DA–UA, showed very good recovery for DA. Consequently, researchers observed the quantitative recovery of DA from the real samples of the bovine serum spiked with DA and detected it in the concentrated DA injection solution. They confirmed the validity of this new SWV in comparison to the earlier potentio-dynamic technique with a caffeic acid-modified-GC electrode.[68]

In their study, Deiminiat and Rounaghi used CV and proposed a method to measure ketamine using a one-step electropolymerization of the MIP with the polytyramine (pty), sol–gel, functionalized MWCNTs@Au NPs (fMWCNTs@AuNPs) nano-composite and ketamine on a pencil graphite electrode (PGE). They entrapped the f-MWCNTs@AuNPs nanocomposite in the polymer network to augment the rate of the electron transfer and their sensor sensitivity. After that, the chemical reduction technique was used to synthesize the f-MWCNTs@AuNPs nanocomposite. Electrochemical impedance spectroscopy (EIS), SWV, and CV were employed to examine the electrochemical behaviors of the modified electrode. Based on the optimal testing condition, a calibration curve of the MIP electrode was drawn and 2 dynamic linear ranges of 1.0–50.0 nM, and 50.0–1000.0 nM, and the LOD of 0.7 nM were observed for quantitatively measuring ketamine in the solution. These outputs showed very good stability, suitable iterability and reproducibility, and higher selectivity and sensitivity of this new sensor toward ketamine molecules. The researchers demonstrated the successful utilization of the

electrochemically imprinted sensor to determine ketamine in biological samples with reasonable outputs.[69]

Another study dealt with the fabrication of a strongly sensitive voltammetric sensor for caffeine (CF) and aspirin (ASA) on a GCE modified with a composite film of MWCNT and poly(4-vinylpyridine) (P4VP). According to the CV of P4VP–MWCNT/GCE, the reaction of the electrode was one of the usual diffusion-limiting processes and the CF and ASA catalytic reactions were observed in 0.1 M PB (pH of 7.4). In order to detect ASA, a 30-fold enhancement was found in the anodic peak current (I_{pa}) at P4VP–MWCNT/GCE in comparison with the bare GCE. It was shown that at the optimal parameters, I_{pa} linearly depended on the CF (2.0–200 μM) and ASA (0.04–350 μM) concentrations. Moreover, the respective LODs of CF and ASA equaled 1.19 nM and 4.42 nM. They used DPV to determine CF and ASA in the presence of paracetamol (PCT) and revealed that it is possible to assay ASA in the biological samples without any interference from PCT and CF. Furthermore, this P4VP–MWCNT/GCE showed acceptable stability, recovery, and reproducibility in the biological and drug samples.[70]

The electropolymerization of a poly(sulfo-salicylic acid) film on a gold electrode modified by 2-mercapto-benzothiazole self-assembled monolayer and MCNTs (PSSA/CNTs/MBT/Au) was performed by Arvand and co-workers.[71] Other researchers used their sensor to determine rutin (Fig. 5) and the electrocatalytic activities of the resultant sensor toward rutin oxidation were ascribed to the presence of the PSSA/MWCNTs nanocomposite. Based on the optimal conditions, a LOD of 1.8 nM and 2 linear calibration ranges from 0.01–0.8 to 0.8–10.0 μM were observed for the detection of rutin at the PSSA/CNTs/MBT/Au electrode. Consequently, the successful application of this electrode to determine rutin in the samples of red onion, red apple, orange,
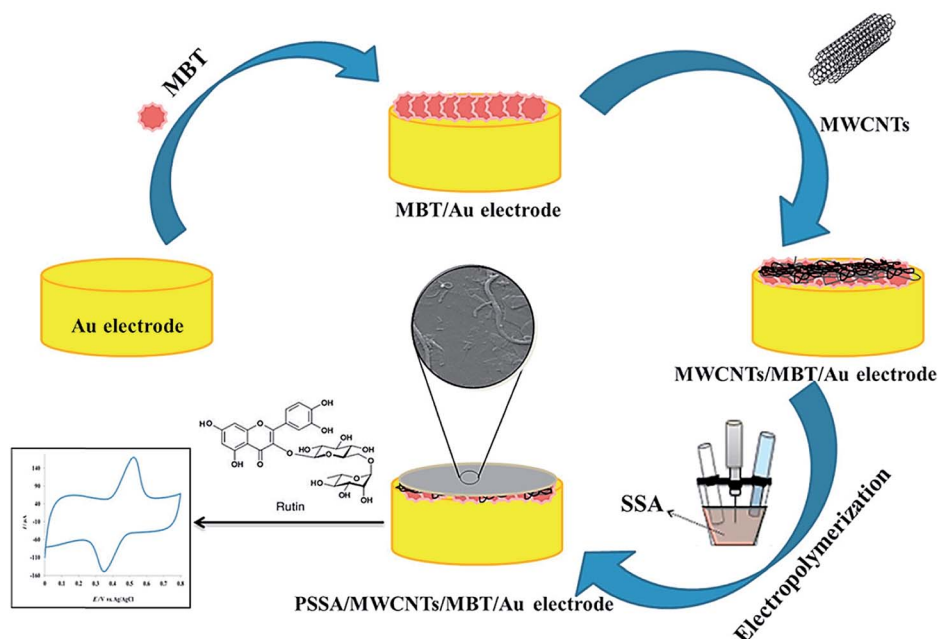

Fig. 5 The preparation process of the PSSA/CNTs/MBT/Au-modified electrode for rutin sensing. Reproduced with permission from ref. 71. Copyright 2018 Elsevier.

strawberry, salvia, and oat was achieved. This electrode presented several advantages, such as high repeatability, reproducibility, and great stability, with its probable use for the fast, sensitive, and selective detection of rutin.[71] Table 1 presents some features of the conducting polymer-based sensors to determine diverse medicines.

4.1.2. Environmental pollution analysis. Braik et al. used superoxide dismutase and incorporated the MWCNTs with the conducting polymer poly(3,4-ethylene-dioxythiophene) (PEDOT) in diverse configurations to devise a new strongly-sensitive electrochemical biosensor for directly determining the superoxide (O_2^-) reactive oxygen species.[72] When the materials were characterized, researchers optimized the experimental conditions and specified the analytical variables of superoxide dismutase biosensors based on the PEDOT/CNT or CNT/PEDOT-modified GCE and those with just one component (MWCNT, PEDOT). The most acceptable analytical function was shown by the biosensor containing the CNTs on the top of PEDOT, which was caused by the synergistic impacts with the rapid and selective responses to O_2^-, the higher sensitivity of ~1115 μA cm^{-2} mM^{-1} and lower LOD of 1 μM, which have been utilized for determining the antioxidant capacity of beverages. This biosensor displayed considerable stability within 2 months and slightly increased the initial sensitivity.[72]

Cui et al. designed a precise, sensitive, electrochemical sensing method for H_2O_2 levels, without oxygen interference, which has been considered as one of the prominent parameters in the environmental, clinical, and biological areas. They modified a boron-doped diamond (BDD) electrode using mesoporous platinum (MPrPt) via the electrodeposition of the Pt–Cu alloy and the anodic dissolution of Cu from the alloy and electropolymerization of the PPy (PPy3C : PPy = 4 : 1, molar ratio) co-polymer and a poly(pyrrole-3-carboxylic acid) (PPy3C). The analyses indicated the greater roughness factor of the resultant Pt and the more efficient surface area of the MPrPt/BDD, as well as the smaller resistance of the charge transfer in comparison to the ones in the Pt NPs-modified BDD electrode. The PPy3C–PPy/MPrPt/BDD electrode displayed a highly selective, sensitive, exact, reproducible, stable, and wider linear range of H_2O_2 response at the neutral pH based on ambient conditions with the same sensitivity and S/N ratio as the ones in

control of nitrogen. Cui et al. revealed a 2 μM LOD for H_2O_2 with the linear range between 5 μM and 49 mM (4 orders of magnitude). It was found that MPrPt, PPy3C–PPy copolymer, and the BDD substrate had a synergic impact on the significant sensing function. The determination did not show any endogenous oxygen interferences of concern in the microanalysis, in vivo monitoring, and field utilizations.[73]

Harraz et al. demonstrated the synthesis of a new nanocomposite of α-Fe$_2$O$_3$/cross-linked PANI (α-Fe$_2$O$_3$/CPANI) through the simultaneous detection of the gelation and polymerization procedures. Therefore, researchers utilized the α-Fe$_2$O$_3$/CPANI nanocomposite as an effective hydrazine chemical sensor with greater selectivity and sensitivity. The electrochemical determination of hydrazine was performed at the α-Fe$_2$O$_3$/CPANI-modified GCE by CV and amperometry and then compared with the bare GCE or pure α-Fe$_2$O$_3$. The schematic representation of the synthesis of the α-Fe$_2$O$_3$/CPANI nanocomposite and the amperometric detection of hydrazine are shown in Fig. 6.

On comparison to the pure α-Fe$_2$O$_3$ or bare GCE, the α-Fe$_2$O$_3$/CPANI nano-composite-modified GCE showed a more acceptable sensing function with the sensitivity of 1.93 μA μM^{-1} cm^{-2}, 0.153 μM LOD at (S/N = 3), a wider linear range of hydrazine concentration between 0.2 μM and 40 μM, a correlation coefficient (R^2) of 0.9983, and a response time of <12 s. This α-Fe$_2$O$_3$/CPANI-modified electrode exhibited electrochemical stability and higher selectivity as a trivial cross-sensitivity to the conventional bioactive interfering samples, and numerous metal ions have been reported.[74]

In another study, Liu et al. presented a poly(aniline-co-o-aminophenol)-modified GCE (PAOA/GCE) for aqueous nitrite detection. PAOA showed stable redox activities and conductivities in wider pH ranges than PANI, which made it appropriate for use as the electrode material in a neutral medium. Researchers used the electrochemical co-polymerization of aniline and o-aminophenol to prepare PAOA/GCE. FT-IR and SEM outputs confirmed PAOA formation and the electrode displayed a greater response towards nitrite oxidation in comparison to the PANI-modified GCE and the bare GCE. Furthermore, researchers determined the impacts of the rate of scan, temperature, and pH on the determination of nitrite.

Table 1 Some validation variables for conducting polymer-based sensors for the detection of diverse medicines

| Electrochemical sensor	Method	Analyte	Detection limit	Linear range	Ref.
MIP/GCE	DPV	Streptomycin	0.5 nM	2.0–1000.0 nM	63
MIP/AuNP-PEDOT:PSS/SPCE	DPV	Nitrofurantoin	0.1 nM	1.0–1000.0 nM	64
GR/p-AHNSA/SPCs	SWV	Dopamine	2 nM	0.05–100.0 μM	65
		5-Hydroxytryptamine	3 nM	0.05–150.0 μM	
PANI–Ni/SPCE	Amperometric	Ascorbic acid	0.62 μM	2.0–1210.0 μM	66
SPCE/PEDOT/GO	Amperometric	Clenbuterol	0.196 ng mL^{-1}	5.0–150.0 ng mL^{-1}	67
DA imprinted-GC/P(Cz-co-ANI)-Aunano	SWV	Dopamine	2.0×10^{-6} M	10^{-4} to 10^{-5} M	68
Polytyramine/sol–gel/f-MWCNT@AuNPs MIP/PGE	SWV	Ketamine	7×10^{-4} μM	1.0×10^{-3} to 1.0 μM	69
P4VP–MWCNT/GCE	DPV	Aspirin	4.42 nM	0.04–350.0 μM	70
		Caffeine	1.19 nM	2.0–200.0 μM	
PSSA/MWCNTs/MBT/Au	DPV	Rutin	1.8 nM	0.01–10.0 μM	71
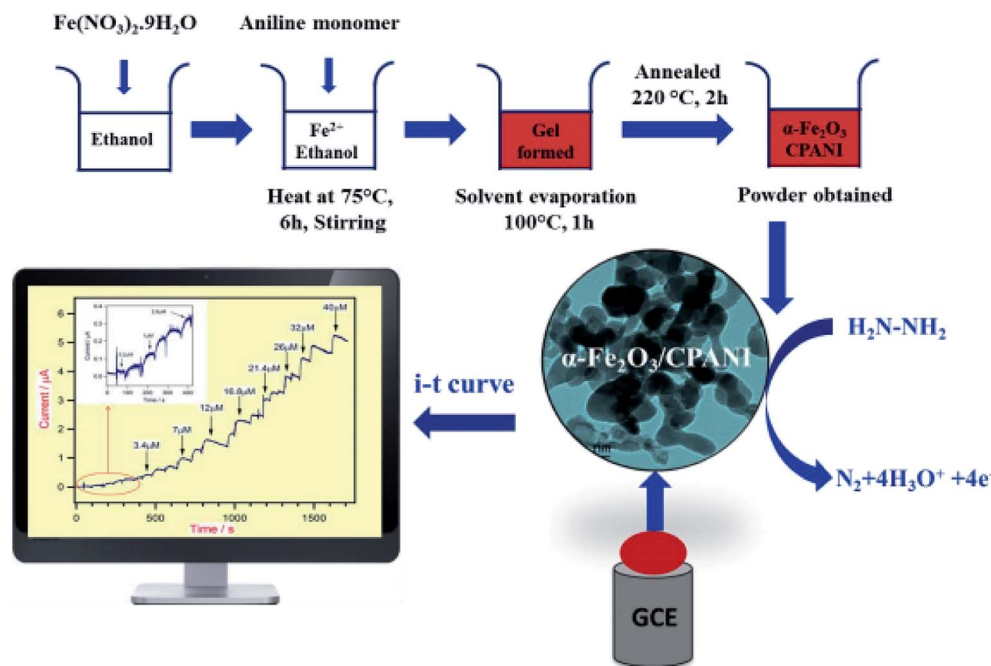
Fig. 6 Schematic representation of the synthesis of the α-Fe₂O₃/CPANI-modified GCE, along with the amperometric detection of hydrazine. Reproduced with permission from ref. 74. Copyright 2016 Elsevier.

Consequently, it was possible to use PAOA/GCE in the wider pH-range between 2 and 8 and determine nitrite in a linear range between 5.0×10^{-6} and 2.0×10^{-3} M with 2×10^{-6} M LOD. Therefore, the electrode had very good stability, anti-interference abilities, and reproducibility, reflecting its attractiveness in the detection of aqueous nitrite in drinking water and ground water.[75]

Wang *et al.* presented a sensitive electroanalytical procedure for detecting trace amounts of Cu^{2+} by means of the phytate-functionalized PPy nanowires (PPyNWs)-modified GCE. Electrostatic absorption and ultrasonic mixing were used to prepare phytic acid/PPy (PA/PPy) NWs. The findings revealed that the PA/PPy NWs-modified GCEs and PPy NWs had electrochemical responses towards Cu^{2+}. As a result of the synergistic impacts between PPy NWs and PA, the PA/PPy NWs-modified electrode displayed greater sensitivity as compared to that of the PPy NWs-modified electrode. Moreover, the PA/PPy NWs composite-functionalized electrodes had a suitable linear association with Cu^{2+} in the concentration range between 10 and 60 μg L⁻¹ and LOD of 3.33 μg L⁻¹ (S/N = 3). Consequently, the researchers utilized the electrochemical sensor for assaying Cu^{2+} in real water samples.[76]

Zuo *et al.* electrochemically determined Hg^{2+} at the trace level based on the poly(3,4-ethylenedioxythiophene) nanorods/graphene oxide nano-composite-modified GCE (PEDOT/GO/GCE). The researchers introduced this PEDOT/GO nano-composite using a simplified liquid–liquid interfacial polymerization method. Moreover, they used DPSV for determining low concentrations of Hg^{2+} on the PEDOT/GO/GCE. Then, they optimized the experimental condition like the accumulation time, deposition potential, and pH-values and based on the

optimum conditions, the peak current was linearly related to the Hg^{2+} concentration in the 10.0 nM to 3.0 mM range. The analysis showed a 2.78 nM LOD at the signal to noise ratio of 3; ultimately, the outputs reflected the successful utilization for Hg^{2+} detection in the tap water samples.[77]

In one of the studies in the field, Selvan *et al.* in 2018 addressed the synthesis of the graphite electrodes coated with a CNT/asymmetrical N₄ tetradentate Schiff base-ligand *N,N′*-bis(pyrrole-2-yl-methylene)-2-amino-benzylamine *via* condensing 2-amino-benzylamine. Then, pyrrole-2-carboxaldehyde was examined as one of the electrochemical sensors for simultaneously determining Hg(II) and Pb(II) in 0.1 M acetate buffer at the pH of 4.5 (Fig. 3). SWASV was used to investigate the electrochemical response features of the modified electrode toward Hg(II), as well as the Pb(II). A series of experiments have been accomplished for finding the best variables of deposition and stripping of the metal ions like deposition time, supporting electrolytes, and pH. Moreover, the linear calibration graph ranged between 3.3 and 66 nM Pb(II) ions and Hg(II) metal ions. The LOD was 0.36 nM for Hg(II) and 1.1 nM for Pb(II) (S/N = 3). Finally, researchers experienced the successful utilization of their sensor for determining Hg(II) and Pb(II) in real samples with acceptable recovery (Fig. 7).[78]

A strongly sensitive electrochemical aptasensor based on electropolymerized poly(pyrrolenitrilotriacetic) acid film and a novel aptamer functionalized with a penta-histidine peptide to quantify bisphenol A was designed by Kazane *et al.*[79] The electrochemical signal of the $[RuIII(NH_3)_6]^{3+}$ complex bound by the electrostatic interaction over the aptamer-modified electrode was used to estimate the surface coverage of the anti-bisphenol A aptamer of 1.84×10^{-10} mol cm⁻². The binding

Fig. 7 Fabrication procedure for the electrochemical sensor for the simultaneous determination of Hg(II) and Pb(II). Reproduced with permission from ref. 78. Copyright 2018 Elsevier.

of bisphenol A over the polymer film has been substantially described by the electrochemical techniques of SWV and EIS measurements. Therefore, the introduced label-free impedimetric aptasensor had a wide linear range from 10^{-11} to 10^{-6} M with 372 Ω sensitivity per unit of the log of concentration and a very good specificity towards the interfering parameters like 4,4′-dihydroxy-biphenyl and bisphenol P.

In their study, Sadriu et al. addressed the electrochemical synthesis of the isoproturon-imprinted PPy films over the GC electrodes in the ethanol and aqueous solution of pyrrole as a monomer, isoproturon as a template molecule, and LiClO$_4$ as the supporting electrolyte (Fig. 4). CV and chrono-amperometry were used to run electro-polymerization. Moreover, the successful entrapment of the isoproturon template molecules was reported in PPy film, where they provided artificial recognition cavities. Following the electrochemical extraction of the template, the PPy film functioned as a MIP for selectively detecting isoproturon while the non-imprinted polymer (NIP) film that was constructed under similar conditions, except for the presence of isoproturon, had no interactions. CV was used to characterize the NIP and MIP films in the presence of the redox probes. EQCM (Electrochemical Quartz Crystal Micro-balance) was used to estimate the polymer layer thickness and Faraday's law was used to calculate it. The analyses showed the isoproturon-selective determination even in the presence of carbamazepine and carbendazim interferents using the isoproturon-imprinted PPy films. In the next stage, the researchers utilized SWV to determine the LOD of 0.5 μg L^{-1} in

milli Q water, whereas the LOD in the real water samples was 2.2 μg L^{-1} (Fig. 8).[80]

Kaur et al. presented one of the nano-composites containing the conducting polymer (CP)–poly(3,4-ethylene-dioxythiophene) (PEDOT) and MWCNT with electrochemical deposition over the surface of the fluorine-doped tin oxide (FTO) to analyze malathion organophosphate (OP); –COOH functionalization of the MWCNTs was performed to covalently immobilize the enzyme acetylcholinesterase (AChE). FE-SEM, FTIR, and electrochemical investigations were used to procure the provided AChE/PEDOT-MWCNTs/FTO as well as PEDOT-MWCNTs/FTO bioelectrodes. Moreover, diverse optimization investigations were accomplished for distinct variables like the pH of 0.1 M phosphate buffer solution (PBS) (7.5), substrate concentration (0.3 mM), inhibition time (10 min), and AChE concentration (50 mU). Analyses showed a 1 fM LOD in the linear range between 1 fM and 1 μM so that it was possible to regenerate the inhibited AChE to 99% by 2-PAM. Consequently, the storage stability and re-usability of the procured bioelectrode were 30 days and 7 times, respectively. The recovery of the malathion from the spiked lettuce sample ranged from 96% to 98% on employing the designed bio-electrode.[81] Table 2 presents some features of the conducting polymer-based sensors for determining diverse environmental contamination.

4.1.3. Food analysis. Xu et al. utilized the hydrothermal procedure to prepare the MoS$_2$/graphene-carbon nanotubes (MoS$_2$/GN-CNTs) nanocomposite. This nanocomposite combined the higher catalysis of MoS$_2$ with the better electronic conductivity of GN-CNTs and displayed higher electrochemical

Synthesis of the MIP - GC
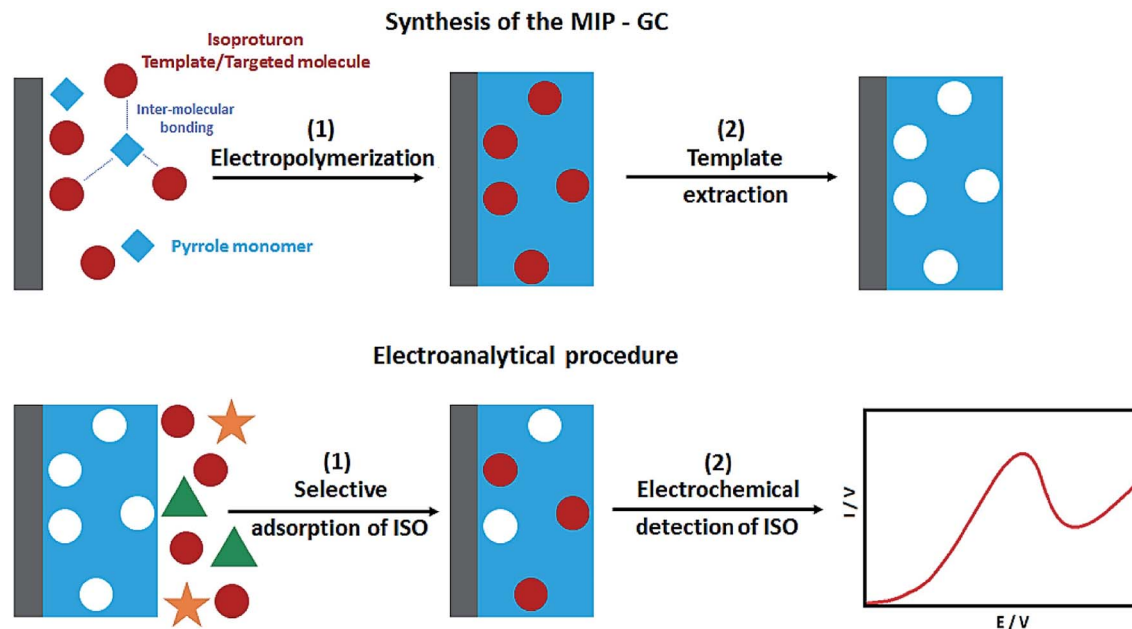

Electroanalytical procedure

Fig. 8 The process applied to the preparation of the imprinted PPy films on the GC substrate MIPGC and isoproturon electroanalysis. Reproduced with permission from ref. 80. Copyright 2020 Elsevier.

sensitivity toward luteolin. MIP film deposited by electro-polymerization based on the carbazole monomer and luteolin template was used to increase the selectivity. Analysis indicated the higher performances of the resultant electrochemical sensor MIP/MoS$_2$/GN-CNTs/GCE. Moreover, the LOD as well as the linear detection range equaled 9.0 nM and 0.040–2.0 mM (S/N = 3), whereas sensitivity equaled 381.3 mA mM^{-1} cm^{-2}. The results demonstrated that there was no interference from 1000-fold concentrations of K$^+$, Na$^+$, Cl$^-$, Ca^{2+}, NO$_3^-$, Mg^{2+}, SO$_4^{2-}$, CO$_3^{2-}$, 500-fold concentrations of glucose and mannitol, 250-fold concentrations of cysteine, lysine, glycine, oxalic acid, and citric acid, and 100-fold concentrations of urea, DA, and ascorbic acid with luteolin detection. Furthermore, 5-fold concentrations of the analogs rutin, naringenin, and catechin and 2-fold quercetin, morin, and kaempferide had no impact on the detection. As a result, the researchers employed their sensor for determining luteolin in the samples of carrot and chrysanthemum tea with compatible outputs to the findings observed in high-performance liquid chromatography.[82]

Gu *et al.* devised a label-free electrochemical impedimetric immunosensor for monitoring melamine, which was substantially utilized to detect melamine in the spiked dairy samples. Researchers observed the co-electrodeposition of poly(pyrrole-*co*-pyrrole-1-propionic acid) and the rGO polymer layer (rGO–PPYPPA) on the electrode with a one-pot procedure and obtained a co-polymer layer with desirable electrochemical features. Then, they applied one of the competitive immuno-assays to quantitatively analyze melamine. This rGO–PPYPPA copolymer ameliorated the conductivity of the sensor and created sufficient anchoring sites to bind antibodies and enhance immunobinding. Notably, certain immune interactions at the electrode surface, which restricted the transfer of the electrons of the redox probe Fe(CN)$_6^{3-/4-}$, changed the electrochemical impedance. These alterations in the impedance were associated with the specific concentration of melamine.

Table 2 Some validation variables of the conducting polymer–based sensors for determining diverse environmental contamination

Electrochemical Sensor	Method	Analyte	Detection limit	Linear range	Ref.
SOD/CNT/PEDOT/GCE	Amperometric	Superoxide	1 µM	20.0–3000.0 µM	72
PPy3C-PPy/MPrPt/BDD	Amperometric	H$_2$O$_2$	2 µM	5.0 µM to 49.0 mM	73
α-Fe$_2$O$_3$/CPANI modified GCE	Amperometric	Hydrazine	0.153 µM	0.2–40.0 µM	74
PAOA/GCE	LSV	Nitrite	2×10^{-6} M	5.0×10^{-6} to 2.0×10^{-3} M	75
PA/PPy/GCE	DNPV	Cu^{2+}	3.33 µg·L.$^{-1}$	10–60 µg L^{-1}	76
PEDOT/GO/GCE	DPSV	Hg^{2+}	2.78 nM	10.0 nM to 3.0 mM	77
CNT/(H$_2$pyrabza) ligand	SWASV	Pb(II)	1.1 nM	3.3–66.0 nM	78
		Hg(II)	0.36 nM	3.3–66.0 nM	
Aptamer-modified electrode	SWV	Bisphenol A	10^{-11} mol L^{-1}	10^{-11} to 10^{-6} mol L^{-1}	79
MIP-GC	SWV	Isoproturon	0.5 µg L^{-1}	2.5×10^{-9} to 5×10^{-6} M	80
AChE/PEDOT-MWCNTs/FTO	DPV	Malathion organophosphate	1 fM	1 fM to 1 µM	81

This immuno-sensor displayed wider detection ranges (10^{-11} to 10^{-2} M), lower LOD (1.2×10^{-11} M) and reasonable recovery (84.6 to 100.3%) in the real samples. The outputs provided a simplified flexible impedimetric immunosensing ground with greater potential for real-world applications.[83]

Consequently, Gursoy et al. prepared an appropriate co-polymer of poly-pyrrole and poly(3,4-ethylene-dioxythiophene) synthesized by the electropolymerization procedure and devised a novel lactose biosensor. Researchers observed the deposition of pyrrole and 3,4-ethylene-dioxythiophene monomers in the presence of sodium dodecyl-benzene sulphonic acid on a platinum disc electrode that was utilized as a working electrode. This sensor was based on the serial reaction of galactose oxidase and b-galactosidase immobilized on the co-polymer-modified platinum disc electrode. SEM, electrochemical analyses, and FTIR spectrometry were utilized to confirm the successful synthesis of the enzyme-immobilized copolymer. CV at 10.40 V was applied to determine the responses of the enzyme electrode to lactose. The bio-sensor response time was in the range between 8 and 10 s and the upper limit of the linear working segment was at a lactose concentration of 2.30 mM with 1.4×10^{-5} M LOD. Furthermore, the Michaelis–Menten constant equaled 0.65 mM of lactose. According to the outputs, this new biosensor had remarkable potential for determining the concentration of lactose in milk.[84]

Researchers modified a commercially available SPCE with the MWCNTs, AuNPs, as well as the poly-neutral red (PNR) film. Afterwards, the electrode was modified with the alcohol dehydrogenase (ADH) for use in the procurement process of the disposable amperometric biosensor to analyze ethanol. Alterations in the current intensity in the amperometric determination of ethanol have been measured to investigate the impacts of diverse modifications applied to SPCE on its electrochemical biosensor features towards ethanol. The alterations have been ascribed to the modifications of the conductivity and electrocatalytic activities of the electrodes. The researchers examined the bio-sensor responses for ethanol as a function of pH, working potential, and amounts of ADH and NAD$^+$. The optimal values of the factors in the ethanol detection equaled 7.75 for pH, 150 units for the amounts of enzyme, +0.2 V for the working potential, and 7 mM for the amounts of coenzyme. Researchers also observed a sensitivity of 0.49 μA mM^{-1}, a linear range of 320.2 to 1000 μM, and LOQ of 96.1 and 320.2 μM for the biosensor. Furthermore, they investigated the biosensor repeatability at +0.2 V with 400 μM ethanol solution. Consequently, 1.57% ($n = 10$) RSD was observed. According to the operational stability investigations, the initial amperometric responses of the biosensor to ethanol declined by 72.2% on day 7. As a result, according to the storage life examinations, the sensitivity of the biosensor diminished by 78.3% at the end of week 6. Next, researchers experimented this new biosensor to detect ethanol in the commercial alcoholic beverages so that the outputs were consistent with the results approved by the pertinent suppliers.[85]

A very simple and selective polymer film-modified electrode for vanillin determination in commercial food products was developed via electrochemical polymerization and over-oxidation of pyrrole by Karabiberoğlu et al. The formation of both poly(pyrrole) and overoxidized poly(pyrrole) films on a glassy carbon electrode surface was characterized by electrochemical impedance spectroscopy, SEM, and X-ray photoelectron spectroscopy. Under the optimized conditions, the calibration graph was comprised of two linear segments of 0.032–1.50 μM and 3.0–150.0 μM with a detection limit of 0.012 μM. The selectivity of the modified electrode was examined in the presence of metals, inorganic ions, and organic substances. Moreover, the proposed method was successfully used for the assessment of vanillin contents in commercial food products with satisfactory results.[86]

4.1.4. Medical diagnosis. One of the novel amperometric xanthine (X) biosensors has been made by Dervisevic and colleagues using the immobilization of the xanthine oxidase (XO$_x$) on the pencil graphite electrode (PGE). They observed the immobilization of xanthine oxidase by glutaraldehyde on the electrochemically polymerized conducting polymer film. Notably, xanthine was detected based on the content used because of the enzymatic reaction of xanthine oxidase. Therefore, they examined the impact of the polymer thickness, the applied potential, temperature, and pH and showed optimal factors to be 5 cycles, +5 V, +0.5 V and 30 °C. Then, they examined the storage stability, the effect of the interfering materials on the amperometric responses, and the operation stability of the enzyme electrode. The LOD and sensitivity were 0.074 μM and 124 mA M^{-1} (S/N = 3), respectively. To verify the new biosensor usability, the electrode was utilized for the measurement of the xanthine concentrations in chicken meat samples.[87]

In this regard, Mudila et al. used redox cyclic voltammetric analysis to explain the efficacious detection of urea, for which a modified PPy graphene oxide (PPY-GO, GO 20% w/w of PPY) nanocomposite electrode was designed. CV measurements indicated the efficient transfer of electrons in 0.1 M KOH electrolytic solution within the potential window range between 0 and 0.6 V. According to the analysis, the PPY-GO-modified electrode had a moderate electrocatalytic impact on the urea oxidation, which resulted in its detection in the electrolytic solution. Researchers utilized SWV in a concentration range of urea from 0.5–3.0 μM with 0.27 μM LOD to determine the current linear dependence versus the urea concentration. Finally, the nanocomposite film-modified electrode applied a synergistic impact like higher conductivity, a faster rate of electron transfer, and intrinsic catalytic abilities.[88]

Kausaite Minkstimiene et al. devised an amperometric glucose biosensor based on the graphite rod (GR) working electrode modified with the bio-composite containing the poly(pyrrole-2-carboxylic acid) (PCPy) particles and then the glucose oxidase (GO$_x$) was examined. PCPy particles were synthesized using chemical oxidative polymerization with H$_2$O$_2$ as the initiator of the polymerization reaction, and were modified covalently with GO$_x$ (PCPy–GO$_x$) following the activation of the carboxyl groups situated at the surface of the particles with a mixture of N-(3-dimethyl-aminopropyl)-N'ethylcarbodiimide hydrochloride (EDC) and N-hydroxy-succinimide (NHS). After

that, the PCPy–GO$_x$ biocomposite was dispersed in a buffer solution that contained specific amounts of bovine serum albumin (BSA). The resultant biocomposite suspension was absorbed on the GR electrode surface, and then solvent airing and chemical cross-linking of the proteins were carried out with the glutaraldehyde vapor (GR/PCPy–GO$_x$). According to the analyses, the current response of the GR/PCPy–GO$_x$ electrode to glucose gauged at +300 mV *vs.* Cl reference electrode was affected by the time interval of the synthesis of the PCPy particles, the pH of the GO$_x$ solution utilized for the modification of the PCPy particles, as well as the amounts of immobilized PCPy–GO$_x$ biocomposite. Moreover, the optimum pH of the buffer solution for activating the biosensor was 8.0. The LOD was 0.039 mmol L^{-1} with regard to the signal-to-noise ratio (S/N: 3), and this glucose biosensor was used to test human serum samples.[89]

Al-Sagur *et al.* published a measurable synthesis of the multifunctional conducting polyacrylic acid (PAA) hydrogel (MFH) integrated with rGO, lutetium phthalocyanine (LuPc$_2$), and vinyl-substituted PANI (VS-PANI) as the powerful 3D matrix for glucose oxidase (GO$_x$) immobilization (PAA-rGO/VS-PANI/LuPc$_2$/GO$_x$-MFH). Researchers then integrated multi-components like PAA with the rGO and VS-PANI *via* a free radical polymerization process with the use of the methylene bis-acrylamide as well as ammonium per-sulfate as the cross-linker and initiator. LuPc$_2$ was doped to form the multifunctional hydrogel (PAArGO/VS-PANI/LuPc$_2$-MFH). Fig. 9A and B respectively indicate the creation of the PAA-rGO/VS-PANI/

LuPc$_2$/GO$_x$-MFH and SEM images of PAA-rGO/VS-PANI-MFH, PAA/VS-PANI-MFH. GO$_x$ was been immobilized in PAA-rGO/VS-PANI/LuPc$_2$-MFH to fabricate the biosensor and utilized for the electrochemical determination of glucose. The PAA-rGO/VS-PANI/LuPc$_2$/GOx-MFH biosensor showed a higher sensitivity of 15.31 μA mM^{-1} cm^{-2} for detecting glucose at concentrations ranging between 2 and 12 mM with LOD of 25 μM. Moreover, the PAA-rGO/VS-PANI/LuPc$_2$-MFH bio-sensor displayed a faster response time (1 s) to the addition of glucose, which had a higher storage stability (three months). According to the real sample analysis, PAA-rGO/VS-PANI/LuPc$_2$/GO$_x$-MFH was efficiently utilized as the electrochemical biosensor in the clinical and industrial diagnosis.[90]

One of the novel selective and sensitive biosensors was presented by Shafaat *et al.* to determine cytochrome C as one of the biomarkers for cell apoptosis. This biosensor has been built based on the electrochemical entrapment of the cytochrome C aptamers in the CPs as the dopant anion on the SPCE surface. EIS, as one of the robust electrochemical techniques, was utilized as a detection technique. This aptasensor showed wider linear dynamic ranges for determining cytochrome C from 10 pM^{-1} nM; 3.29% RSD and 5 pM LOD were seen in the analyses. It also showed higher selectivity and acceptable stability for determining cytochrome C, even in the presence of the serum proteins (such as albumin, lysozyme, fibrinogen, immunoglobulin G) at the increased levels of concentration with success as one of the clinical detection tools for detecting cytochrome C.[91]
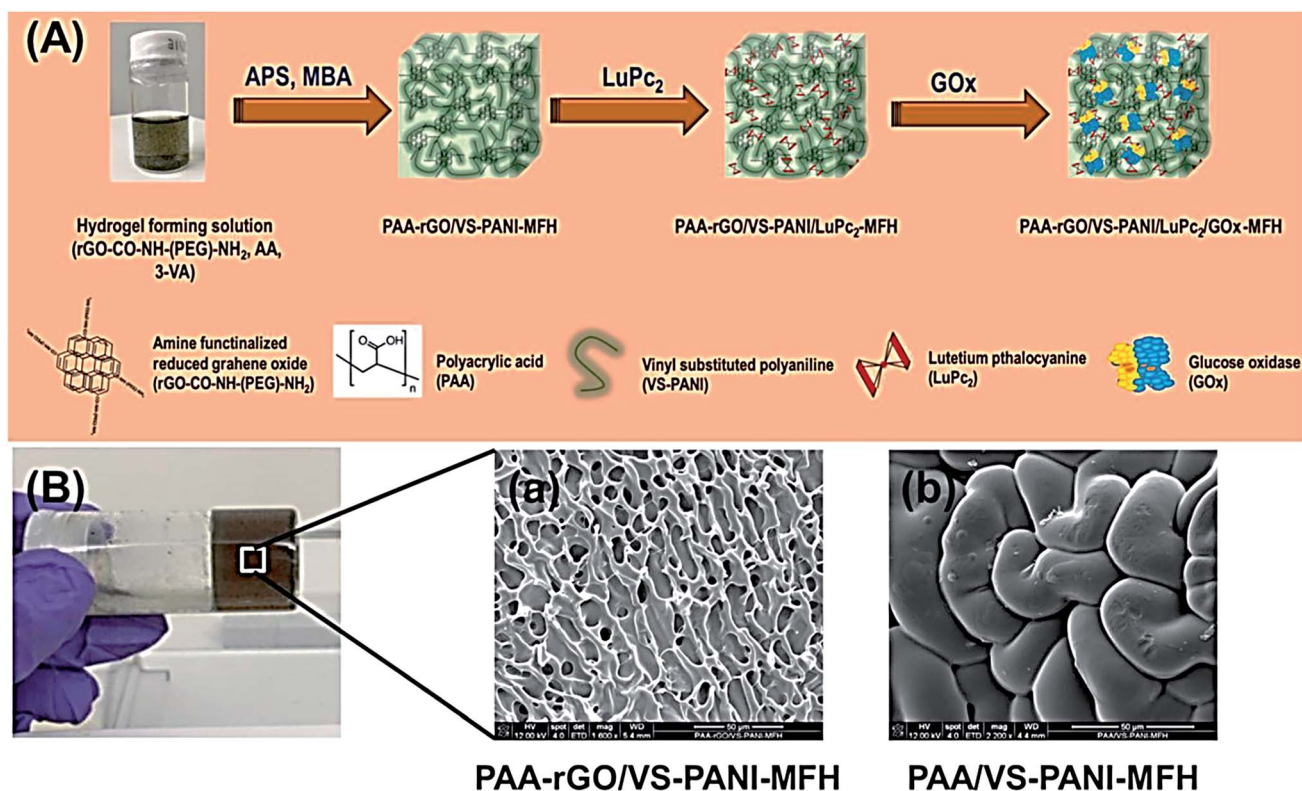

Fig. 9 (A) The PAA–rGO/VS-PANI/LuPc2/GO$_x$-MFH synthesis procedure. (B) SEM images of (a) PAA–rGO/VS-PANI-MFH, and (b) PAA/VS-PANI-MFH. Reproduced with permission from ref. 90. Copyright 2017 Elsevier.

Serafín *et al.* provided a fast, sensitive method for determining the clinically related biomarker receptor tyrosine kinase AXL in the serum consisting of the amperometric disposable immunosensors. Therefore, they sandwiched the targeted protein between a particular capture antibody covalently immobilized on the SPCEs modified with the electro-polymerized poly(pyrrolepropionic acid) and a biotinylated detector antibody labeled with a streptavidin-horseradish peroxidase conjugate. Researchers also measured the amperometric response at -0.20 V *versus* the Ag pseudo-reference electrode of the SPCE by adding H_2O_2 in the presence of hydroquinone (HQ) as the mediator. Such an integrated immuno-sensing platform represented a lower LOD of 337 pg mL^{-1}, acceptable selectivity as compared to the other non-target serum proteins and finally offered outputs with statistical compatibility with the ones observed in the use of a commercial ELISA kit. Hence, it could be said that the mentioned interesting characteristics, simplified operation and automation, and miniaturization of the pertinent equipment made this method an encouraging candidate for developing the tools for on-site clinical analyses.[92]

Kangkamano *et al.* devised a label-free electrochemical miRNA biosensor based on a pyrrolidinyl peptide nucleic acid (acpcPNA)/PPy/silver nanofoam (Ag NF)-modified electrode. This AgNF was electrodeposited as a redox indicator on the gold electrode that was functionalized with an electro-polymerized layer of PPy, which was considered as a conducting polymer, for the immobilization of the PNA probes. EIS was used to investigate the construction procedure of the method. Researchers utilized the biosensor for detecting miRNA-21 that was considered as a biomarker with abnormal expression in several kinds of cancer. They used CV and controlled the signals by changing the current of the Ag NF redox reaction prior to, and following, the hybridization. 2 PNA robe lengths were examined and the longer probe represented the more acceptable function. It was found that nucleotides overhanging on the electrode side had a greater impact on the signal than those on the solution side because of the higher insulation of the sensing surfaces. Based on the optimum conditions, the electrochemical signal was proportionate with the miRNA-21 concentration ranges between 0.20 fM and 1.0 nM, with a lower LOD of 0.20 fM. This biosensor exhibited higher specificity with the ability to differentiate between the complementary single- and double-base mismatched, and non-complementary targets. Analyses showed that 3 of 7 experimental plasma specimens had certain concentrations of 63 ± 4, 111 ± 4, and 164 ± 7 fM. Thus, this sensor exhibited an acceptable recovery of 81–119%. Consequently, the possible analyses of the biosensor without RNA extraction and or amplification showed the potential usefulness of the sensor for the prognosis as well as diagnosis of cancer in clinical applications.[93]

4.2. Energy storage and conversion

Experts in the field have considered energy as the most prominent universal issue because of the exhaustion of fossil fuels. Energy storage devices require electrode materials with good electronic conductivity to deliver maximum power. CPs are very attractive materials due to their broad range of conductivities, from semiconductor (10^{-11} to 10^{-3} S cm^{-1}) to metal (10^{-1} to 10^6 S cm^{-1}) behavior. Their charge storage can be enhanced by controlling the synthetic parameters (*i.e.*, doping agent, temperature, pH, *etc.*) or by designing different morphologies, surface area, redox activity, *etc.* CPs have very high current density and are inexpensive when compared to carbonaceous electrode materials. Taking PANI as an example, a supercapacitor device based on PANI can exhibit a specific energy of 10 W h kg^{-1} with a slightly lower specific power of 2 kW kg^{-1}, while a carbon-based supercapacitor device can only reach a specific power of 3–4 kW kg^{-1} and a specific energy of 3–5 W h kg^{-1}. In particular, CPs are utilized in energy storage devices due to their high charge/discharge cycling rate, high conductivity, large surface area, high specific capacitance, and good redox reversibility.[94,95] The conducting polymers generally have high specific capacitance values and can be desirable materials for developing the next generation of energy storage and conversion.

4.2.1. Supercapacitors. It is widely accepted that super-capacitors have been helpful as the tools of energy storage and could achieve higher capacitance values than the traditional capacitors and higher power density in comparison to the batteries. Researchers have largely considered the super-capacitors (electrochemical capacitor) as a result of their higher power density, acceptable cycle stability, and quicker charge or discharge abilities. Nevertheless, for lessening the overall cost, the charge/discharge rate, energy density, and electrode material of the super-capacitors should be thoroughly adjusted with an affordable high conducting resource. Researchers have also thoroughly investigated conducting polymers like PANI, PPy, PThs, and their derivatives because of the encouraging electrical conductivity and electro-activity.[96–98]

Although experts in the field have found it necessary to the design of the nanostructured poly(3,4 ethylene-dioxythiophene) (PEDOT) with increased capacitance and mechanical flexibility to realize the high-performance supercapacitors, it is hard to make these types of electrodes with fast and affordable methods. Therefore, Wang *et al.* introduced a simplified, rapid, and flexible approach to making the mechanically powerful, strongly conductive, and versatile nanostructured PEDOT paper. The composite substance that could be fabricated in 30 min with the solution-based reactions exhibited a larger surface area (137 m^2 g^{-1}), lower sheet resistance (1.4 Ω cm^{-1}), and higher active mass loading (7.3 mg cm^{-2}). The symmetric PEDOT paper-based super-capacitors provided a higher specific electrode capacitance of 90 F g^{-1}, 920 mF cm^{-2}, and 54 F cm^{-3} and very good cycling stability (93% capacity retention after 15 000 cycles at 30 mA cm^{-2}) in 1.0 M H_2SO_4. The electrochemical function of the supercapacitors was retained at various bending angles, which showed the flexibility of the tools.[99]

He *et al.* demonstrated a simplified poly(*o*-methylaniline)-derived construction of the bifunctional microporous nitrogen-doped carbon micro-spheres (NCMSs) with increased electrocatalytic activities and stability for energy storage and the

oxygen reduction reaction (ORR) in the supercapacitors. It was observed that when the pyrolysis temperature reached 900 °C, the dispersed NCMSs presented a higher surface area of 727.1 m^2 g^{-1}, acceptable total N-doping content, and a higher concentration of the quaternary N, exhibiting a more reasonable electrocatalytic activity for the ORR in comparison to the commercial Pt/C catalysts. The higher specific capacitance (414 F g^{-1}) and very good durability showed their attractiveness for the advanced process of energy conversion and storage; therefore, their conducting polymer-derived method can offer novel ground for making heteroatom-doped carbon substances for energy device applications.[100]

Jena *et al.* addressed a new PANI derivative, poly(2-methyl thioaniline)-coated MWCNTs (PMTA@CNT) and the composite with graphene (PMTA@CNT/RGO) for use as the supercapacitor. The PMTA@CNT/RGO and PMTA@CNT electrodes exhibited considerably greater specific capacitances of 616 F g^{-1} and ~522 F g^{-1} in 6 M KOH electrolyte at a current density of 1 A g^{-1}. The obtained outputs were nearly 28 and 36% greater than the PANI@CNT/RGO and PANI@CNT electrodes procured by a synthesis procedure similar to the PMTA based electrode. It is worth mentioning that the PMTA-based composite electrode had a very good electrochemical function as compared with the PANI-based composite electrode. This could have been caused by the presence of an acceptable electron-donating group (–SCH₃) in PMTA, which made the

PMTA molecule electronically rich *via* the resonance effects that facilitated the transfer of the charges between the 2 components using the π-electrons of the quinoid rings in PMTA and benzenoid rings of the CNTs or graphene (Fig. 10). Hence, the PMTA composite electrode with acceptable capacitive behaviors encouraged its utilization for competing with the PANI composite-based electrode.[101]

Zhu *et al.* simply synthesized N-doped porous carbons (NPCs) with the nano-fiber-like structure by a one-step direct carbonization/KOH activation of the poly(aniline-*co*-p-phenylene-diamine) (P(ANI-*co*-PPDA)) at 600 to 900 °C in a N_2 atmosphere. They showed that the greater heat treatment temperature enhanced the specific surface area (between 776 and 2022 m^2 g^{-1}), whereas it decreased the nitrogen content (from 6.96 to 1.18 wt%). The final NPCs (*i.e.*, NPC-700) showed a higher surface area of 1513 m^2 g^{-1}, higher N content (6.43 wt%), and nanofiber-like morphology at 700 °C. The results indicated that in 6 M KOH electrolyte, the NPC-700 electrode had a capacitance of 316 F g^{-1} at 1.0 A g^{-1} and 167 F g^{-1} at 10.0 A g^{-1}. The NPC-700 electrode exhibited an acceptable cycling stability with 81.6% capacitance retention after 5000 cycles at 1.0 A g^{-1}. Finally, the simplified synthesis path and higher electrochemical functions of NPCs showed higher potential in the supercapacitor application.[102]

Ji *et al.* presented a quaternary electrolyte formulation for constructing a pristine carbon and PPy composite, which did
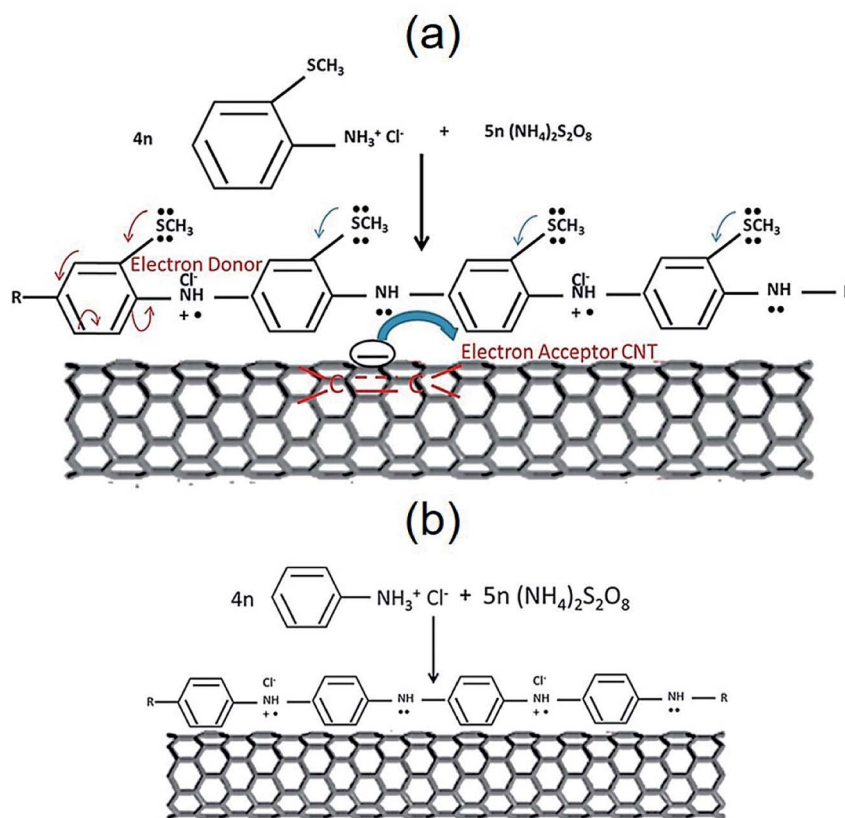

Fig. 10 The electron conjugation process of the SCH₃ group of (a) PMTA *versus* (b) PANI, accompanied by the traditional donor–acceptor state of the interaction (probable conduction mechanism). Reproduced with permission from ref. 101. Copyright 2017 Elsevier.

not sacrifice electron or ion mobility. Lithium perchlorate (20 mM) was used as a supporting electrolyte and dopant, with sodium dodecyl-benzenesulfonate at a lower concentration of 1.43 mM as a surfactant, as well as pyrrole monomers and pristine carbon nanomaterials. Based on the analyses, the difference in the order of magnitude between the concentration of the dopant and surfactant ions allowed the as-deposited PPy to be dominantly doped by the small-sized and mobile perchlorate anions. Researchers succeeded in the preparation of the PPy composites with carbon black, CNTs, and electrochemically exfoliated graphene (EEG) with their newly fabricated quaternary electrolyte. Therefore, this PPy/EEG composite electrode exhibited 348.8 F g^{-1} specific capacitance with higher rate capability (190.7 F g^{-1} at 71 A g^{-1}). Supercapacitor instruments based on the PPy/EEG composite electrodes exhibited higher rate behaviors of 500 mV s^{-1} and a longer cycle life of 5000 cycles.[103]

4.2.2. Solar cells. It is widely accepted that solar cells are energy conversion instruments that convert sunlight into electrical energy. The conducting polymers enjoy specific features of the light adsorbance and hole transport in combination with the metal oxide that can be involved in improving the photovoltaic efficiency.[104,105]

Gal et al. introduced the polyacetylene-based polyelectrolyte for application as quasi-solid-state dye-sensitized solar cells (DSSCs). Researchers used the phosphorus oxychloride activated polymerization of 2-ethynylpyridine to prepare the conjugated polyelectrolyte, and poly[2-ethynyl-N-(dichlorophosphino)pyridinium chloride] was utilized for the DSSC. The photoluminescence (PL) spectrum of the polymer solution demonstrated 2 maximal peaks of 471 and 489 nm relative to the photon energies of 2.64 eV and 2.54 eV. Poly[2-ethynyl-N-(dichloro-phosphino)pyridinium chloride] was used to fabricate the quasi-solid-state DSSCs with a SnO$_2$:F/TiO$_2$/D719 dye/solid-state electrolyte/Pt device, reflecting the highest power conversion efficiency (PCE) of 5.70%.[106]

Gopalan et al. reported the design and synthesis of a novel sulfonated PANI derivative consisting of thiol (−SH) groups
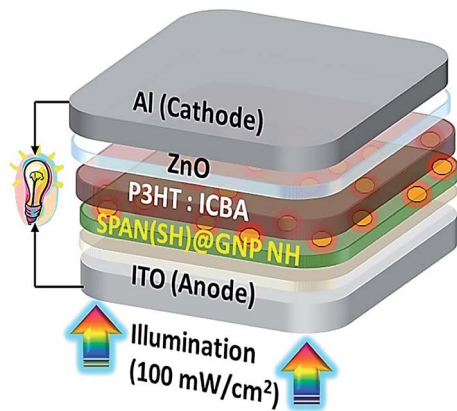

Fig. 11 BHJ PSC with the tool architecture: ITO/SPAN(SH)@GNP(X%) NH/P3HT; ICBA/ZnO/Al. Reproduced with permission from ref. 107. Copyright 2018 Elsevier.

(SPAN(SH)) for achieving the efficient dispersion of the AuNPs in SPAN(SH) (SPAN(SH)@GNP). They also assessed the photovoltaic function of the poly(3-hexylthiophene-2,5-diyl): indene-C60 bisadduct (P3HT:ICBA) for elucidating the contribution of the SPAN(SH)@GNP NH (nanohybrid) buffer layer in the polymer solar cell (PSC) device architecture; ITO (indium tin oxide)/ SPAN(SH) or SPAN(SH)@GNP(X%) NH/zinc oxide (ZnO)/Al (Fig. 11). According to the results, the PCE of the PSC was enhanced using the SPAN(SH)@GNP buffer layer. A buffer layer with 1.66 wt% of GNP based on the weight of SPAN(SH), (ITO/ SPAN(SH)@GNP(1.66%)/P3HT:ICBA/ZnO/Al) highly improved the PCE (5.20%), which was significantly greater than the PCE (4.25%) of SPAN(SH) (ITO/SPAN(SH)/P3HT:ICBA/ZnO/Al). The very strong near field of the GNP was distributed laterally in the buffer layer and extended vertically into the adjacent P3HT:ICBA (active) layer, and provided a greater rate of exciton production in the active layer. Consequently, the synergistic impact of the energy level alignment, lower interfacial resistance, efficient hole extraction, and greater surface areas between the buffer/active layer significantly increased the PCE. Based on the outputs, designing the conducting polymer structure for proper interaction with PNP to achieve greater PCE is of great importance.[107]

Another study conducted by Alem et al. built poly(N-9′-heptadecanyl-2,7-carbazole-alt-5,5-(4′,7′-di-2-thienyl-2′,1′,3′-benzothiadiazole (PCDTBT) based on the photovoltaic cells with the flexographic printing method, enabling the increased throughput-patterned active layers for deposition on the flexible substrates at the lowest cost. Such a condition has been met via the optimization of the flexographic plate pattern, solvent, drying process, and print speed. Researchers also incorporated halftone patterning, which is one of the popular processes in the graphics printing industry, and optimized the speed of printing; therefore, the homogeneity of the active layer print was considerably ameliorated. Future research on the appropriate solvents and drying conditions resulted in better uniformity and lower pin-hole formation. The usability of the flexographically-printed active layer was confirmed by making 1 cm^2 photo-voltaic cells that displayed 3.5% efficiency, which could be compared with the other deposition methods. Hence, the flexography is appropriate for use as one of the construction techniques for bulk heterojunction organic photovoltaics.[108]

One of the device architectures for efficacious perovskite solar cells, which used poly(3-hexylthiophene) as one of the hole transport materials without any dopant, was introduced by Jung and co-workers. A thin layer of the broad-band gap halide perovskite was created on the top of the narrow bandgap light-absorbing layer via an in situ reaction of n-hexyl trimethyl ammonium bromide on the perovskite surface. The new instrument had a strong power conversion efficiency of 22.7% with ±0.51% hysteresis and exhibited suitable stability at 85% relative humidity without any encapsulation. In the case of encapsulation, it demonstrated a lengthier operational stability for 1370 h under 1 sun illumination at room temperature, which maintained 95% of the initial efficiency. Therefore, they extended our platform to the larger area modules (24.97 square centimeters) that have been constructed with a scalable bar-

coating technique for poly(3-hexylthiophene) deposition and reached 16.0% PCE.[109]

It has been demonstrated that the chemical complexity of the conventional DSSC electrolyte required the development of greater selectivity and catalytic counter-electrode (CE) substances for the triiodide target molecule. For example, Sangiorgi *et al.* revealed that the molecularly imprinted PPy (MIP-PPy) could resolve the above problems. Various template molecules like L-2-aminopropionic acid (L-alanine) and 2-aminoacetic acid (glycine) have been investigated in the course of the electro-polymerization procedure for verifying MIP-PPy utilization as CE. Using the lower concentration of glycine resulted in an MIPPPy film that showed greater catalytic activity and electrochemical features on the triiodide reduction in comparison to the non-imprinted PPy (NIP-PPy). Gel-state DSSCs-based on the MIP substances have been procured and tested so that the optimized MIP-PPy CE with glycine as a template displayed nearly 20% enhancement in the power conversion efficiency and 50% reduction in the charge transfer resistance as compared to the cells based-on NIP-PPy. The obtained findings implied the possible enhancement of the PPy CE catalytic features with no addition of other substances or significant modifications in the generation procedure process; however, it enhanced the selectivity of the electrode.[110]

4.2.3. LIB. LIBs have been regarded as major energy storage devices for consumer electronics and also electric vehicles. One of the main principles for LIBs is that Li in the anode materials is oxidized to Li^+ and moves to the cathode where it is inserted in the cathode material. The electrolyte contributes vitally to the LIBs, which creates channels for the ionic charge carrier between the anode and cathode. The key benefits of these LIBs are their being lightweight and their increased energy density; however, they suffer from decreased power, limiting their utilization in several areas, for the electric vehicles in particular.[111,112] Notably, for promoting the electrochemical function of the LIBs, it is necessary to seek proper electrode substances, which are capable of enabling the batteries with the greater intercalated lithium capacity, acceptable lithium deintercalation reversibility, as well as longer cycle life.

Researchers have introduced several CPs with positive effects for improving the rate capability and cycle life of the electrode materials due to their acceptable conductivity (between a few-$S cm^{-1}$ and $500 S cm^{-1}$), faster charge–discharge kinetics, as well as plastic features.[113] Wang *et al.* procured a novel PTh-coated silicon composite anode substance with an *in situ* chemical oxidation polymerization procedure and utilized it as the anode in LIB. They described this substance structure with infrared spectroscopy, proving the occurrence of the oxidative polymerization of thiophene in the α-position. Poly-thiophene offered a more acceptable electric contact between the silicon particles; hence, the as-procured Si/PTh composite electrodes achieved more reasonable cycling performance in comparison to the bare Si anode. Finally, the specific capacity of the composite electrode retained 478 mA h g^{-1} following 50 cycles.[114]

Hua *et al.* designed a new electrodeposited hydrothermal technique for fabricating the high density β-Na0.33V₂O₅ nano-

wire film on the metal current collector (Ti-foil). These researchers investigated the crystal structure, morphology, and impact of the deposition voltage, time, and temperature onto the procured specimens. Analyses showed a thickness of β-Na0.33V₂O₅ nano-wire film of ∼10.5 μm based on the experimental conditions of five hours, 90 °C temperature, and 2.5 V voltage. Coating β-Na0.33V₂O₅ nano-wire film with PPy and using it as a cathode of ILB revealed a higher reversible discharge capacity of 269.9 mA h g^{-1} at a current density of 50 mA g^{-1}. On the contrary, this material cycling behavior has been highly more acceptable than the bare βNa0.33V₂O₅ nano-wire film. Finally, Hua *et al.* provided an interesting ground for exploring higher tap density cathode substances for LIB with greater electrochemical Functions.[115]

Another study conducted by Wang *et al.* designed a new 1D and co-axial PANI@tin dioxide@MWCNT (PANI@SnO₂@-MWCNT) composite as a conductive additive-free anode substance for the LIB. They initially fixed SnO₂ NPs (5 nm) on the conductive MWCNT skeleton *via* self-assembly of the nanosized SnO₂ particles over the MWCNT surface using the surfactant P123 and the *in situ* coating of a flexible layer of PANI with very good conductivity of the electron and lithium-ion (Fig. 12). According to their results, 1D and co-axial PANI@SnO₂@MWCNT has been capable of the effective accommodation of the volume extension of the SnO₂ NPs in the course of the lithiating and de-lithiating by wrapping a flexible coating layer of the PANI and buffer of 1D MWCNT. The synergistic action between MWCNT and PANI ameliorated the electronic and lithium ionic conductivity of the composite. The PANI@SnO₂@MWCNT composite exhibited a lengthier cycling stability and more acceptable rate capability in comparison to the SnO₂@ MWCNT composite, which exhibited a higher reversible charge/discharge specific capacity of 878/888 mA h g^{-1} at 0.2 A g^{-1} over 100 cycles, and 524/527 mA h g^{-1} at 1.0 A g^{-1} over 150 cycles, with no conductive additives in the electrode.[116]

Experts in the field have considerably investigated ZnO as an electrode material in LIBs because of its high theoretical capacity. However, unsuitable electronic conductivity and numerous volumetric alterations in the course of the cycling restrict its industrial utilization. For example, Li *et al.* procured poly-pyrrole nanorings (PNRs) using the solution chemistry technique with pyrrole (Py) as raw material, ammonium persulfate (APS) as the oxidant, and cetyltrimethylammonium bromide (CTAB) as a surfactant. Moreover, zinc oxide NPs adsorbed on the PPy nanoring surface *via* a one-pot *in situ* sol–gel technique have been used to synthesize the ZnO/PNR composite. This composite showed a 3D interconnected network structure where the diameter of the PPy nanorings equals 80–100 nm and the average size of the ZnO nanocrystals with uniform distribution equals 10.49 nm. Therefore, a specific 3D conductive framework could establish suitable electronic contact between ZnO particles and buffer the volume variations in the course of the lithiation or delithiation procedures. The ZnO/PNR composite, as one of the electrode materials for LIBs, provides 1658 mA h g^{-1} first-cycle discharge capacity and 50.7% capacity retention over 150 cycles at 200 mA g^{-1}, which reflects

Fig. 12 The preparation of PANI@SnO₂@MWCNT; steps (1)–(4) represent the dissolution, self-assembly, heating, and *in situ* polymerization. Reproduced with permission from ref. 116. Copyright 2018 Elsevier.

greater specific capacity and the significant stability of the cycle.[117]

4.2.4. Fuel cells. Researchers consider fuel cells as being among the electrochemical devices that provide highly effective and direct conversion of chemical energy into electrical energy by the electrochemical oxidation of hydrogen and small organic molecules like ethanol, methanol, formic acid and other fuels.[118] These cells generate electricity from the external supplies of the fuel (anode side) as well as the oxidant (cathode side) that react in the presence of an electrolyte. Overall, a reactant flows in and the reaction product flows out, whereas the electrolyte maintains its place in the cell. Moreover, the fuel cells are capable of a virtual continuous operation in the case of the maintenance of the essential flows. Therefore, this technology provides an attractive utilization of portable resources of energy and has been considerably investigated.[119–121] These energy-conversion systems need strongly efficacious electrocatalysts for triggering the ORR, which happens at the cathode of the fuel cell. One of the main challenges in this regard would be the design of inexpensive, effective, and stable electrocatalysts for the ORR.[122,123] However, as a result of the respective adjustable conductivity, acceptable electrocatalytic activities, and reasonable electrochemical stability, the conducting polymers are promising electrocatalysts for the ORR.[124] In the early stages, the conducting polymer-based electrodes were made by the direct casting of the neutral conducting polymer/poly(tetrafluoride ethylene) paste on the graphite current collector.[125]

Fard *et al.* built poly(pyrrole-*co*-aniline) (PPCA) hollow nanospheres (HN) as a catalyst support material using *in situ* emulsion polymerization. According to their study, a one-step and template-free strategy was introduced for the fabrication

of the Pd NFs on a PPCA HN-coated GCE using a simplified electrochemical procedure. Moreover, CV, EIS, and chronoamperometry towards the methanol oxidation as one of the model reactions in the alkaline medium have been used to evaluate the catalytic function of the Pd NFs/PPCA HN catalyst. The particular activities of Pd NFs/PPy (1.28 mA cm⁻²), Pd NFs/PPCA HN (1.79 mA cm⁻²), Pd NFs (0.78 mA cm⁻²), and Pd NFs/PANI (0.93 mA cm⁻²) showed that the PPCA-supported Pd NFs with higher surface area exhibited very good electrocatalytic activities in comparison to the other electrodes for the electrooxidation reaction in alkaline medium. Such conditions could be the result of simpler charge transfer at the interface of the conductive copolymer, greater electrochemically available surface areas and electronic conductivity. Therefore, the proposed approach offers encouraging ground for direct methanol fuel cells.[118]

El-Moghny *et al.* recently devised new catalysts of the platinum NPs dispersed on PANi for formic acid electro-oxidation (FAO), which is a basic anodic reaction in the direct formic acid fuel cells (DFAFCs). Fig. 13 depicts the role of PANi in reducing CO poisoning and improving the catalytic activity of the Pt/PANi/GC electrode towards FAO. Therefore, the catalyst preparation scheme allowed the sequential electrodeposition of the fibril PANi and spherical PtNPs (*ca.* 65 nm in size) on the glassy carbon (GC) substrate and permitted the accurate control of the deposition sequence and loading. Moreover, incorporating PANi into the catalyst constituents could considerably (*ca.* 16 times) improve the catalytic activities of the catalyst toward FAO *via* shifting this mechanism toward a suitable dehydrogenation pathway and lessening the unfavorable toxic dehydration pathway. The researchers manipulated the deposition order and loading of diverse constituents of the catalyst to
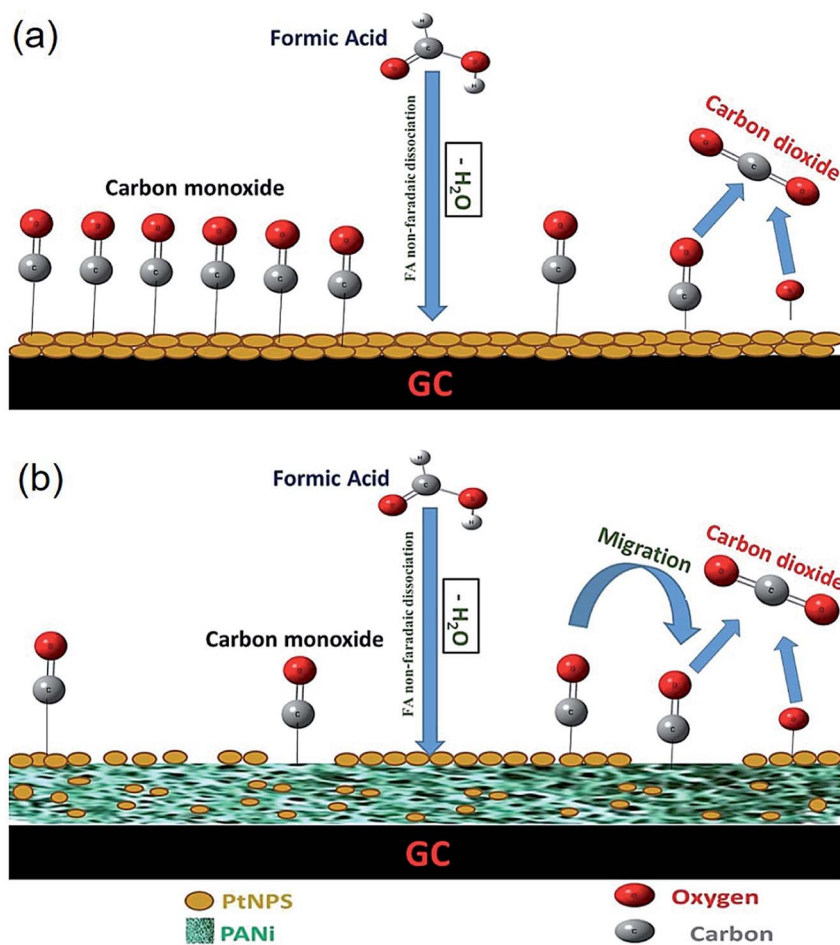
Fig. 13 A representation of the poisoning dehydration pathway of FAO at the (a) Pt/GC and (b) Pt/PANi/GC electrodes. The amount of COads was lowered at the Pt/PANi/GC electrode, and PANi may further preferentially capture CO. Reproduced with permission from ref. 126.

tune the catalytic efficacy. Multiple procedures have been utilized for confirming the substantial deposition of the catalyst and evaluating its composition, morphology, and crystal structure. Although PtNPs would be necessary for absorbing FA, PANi improved the PtNPs dispersion and mediated FAO to facilitate the charge transfer and mitigate the CO toxicity. Longitudinal continual (150 CVs) electrolysis testing demonstrated encouraging catalytic stability.[126]

Another study conducted by Miglbauer et al. demonstrated the versatility of the conducting polymer poly(3,4-ethylene-dioxythiophene) (PEDOT) as an electrocatalyst for the peroxide fuel cells with no loss as a result of disproportionation. The researchers showed that PEDOT, as one of the cathodic catalysts to reduce peroxide to water, performed at a level on par with the most acceptable inorganic catalysts. Therefore, with the use of the PEDOT as the cathode and nickel as the anode material, open circuit potentials are possible in the range between 0.5 and 0.6 V with a power density of 0.20–0.30 mW cm^{-2}. Thus, PEDOT functioning as the catalyst for the reduction of the hydrogen peroxide to water can be mechanistically understood. The resulting output would be a measurable hydrogen peroxide fuel cell cathode, used for the demonstration

of the ability of the organic semiconducting substances as the electrocatalysts.[127]

Attar et al. were the first to demonstrate the electrocatalytic function of the PPy–copper oxide particles-modified carbon paste electrode (Cu$_2$O/PPy/CPE) for the electrocatalytic oxidation of ethanol in alkaline media (Fig. 14). They procured the composite Cu$_2$O/PPy with a simplified strategy containing the PPy film deposition on the CPE through a galvanostatic state, followed by the copper particles deposition at a fixed potential. Therefore, researchers applied CV and EIS for characterizing the electrochemical features of Cu$_2$O/PPy/CPE and explaining the electro-oxidation system of ethanol. Attar et al. then examined and optimized the experimental variables affecting ethanol electro-oxidation. Based on the results, the electro-deposition of the copper particles on the PPy film augmented the catalytic activities toward ethanol oxidation, with the peak current density of 2.25 mA cm^2 at 0.8 V vs. Ag/AgCl, which is 2.6 times greater than the peak current density observed in the PPy/CPE electrode. The saturation limit reached a value of 5 M. The acceptable catalytic activity, simplified procurement, and stability of the Cu$_2$O/PPy composite indicate that it is a very good electrocatalyst for the oxidation of ethanol.[128–131]
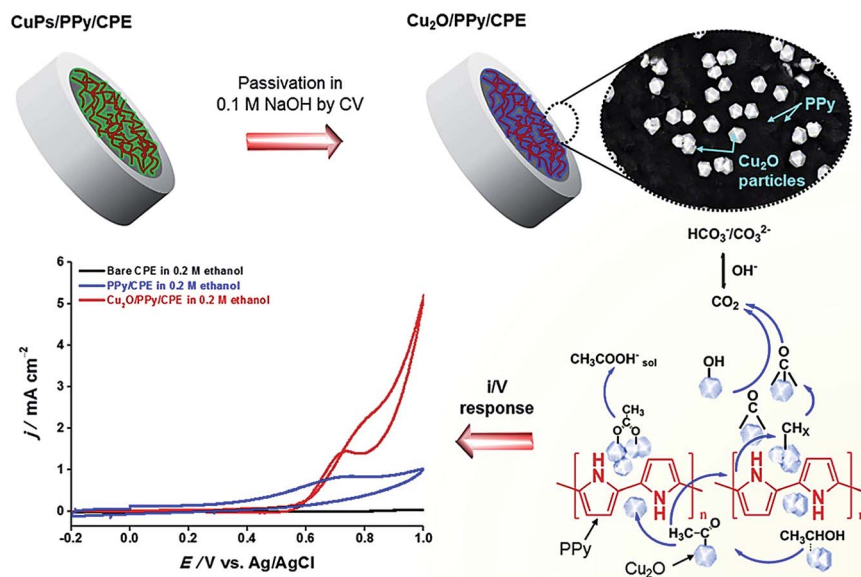
Fig. 14 The preparation of Cu_2O/PPy/CPE for ethanol electrocatalytic oxidation. Reproduced with permission from ref. 128. Copyright 2020 Elsevier.

5. Conclusion

The electrochemical sensors and biosensors have been regarded as making a key contribution to diverse areas like medical diagnosis, medicine, environment, and food analyses. It has been revealed that the conducting polymers have an encouraging contribution to the generation of the latest electrochemical biosensors and sensors as a result of their distinct benefits in comparison to other substances. Notably, the recovery time, responsivity, higher selectivity and sensitivity, and reasonable stability contribute to the production of an acceptable sensor and its function. Generally, features of the charge transfer of the conducting polymers due to the existence of a p-conjugated mechanism resulted in the provision of an appropriate carrier for transferring electrons from the redox-active center to the electrode surface.

As mentioned earlier, experts in the energy storage field are giving increasing consideration to electrical vehicles, grid-scale storage, and portable electronics for the optimal utilization of renewable energy resources like solar and wind energies. Therefore, studies on novel technology for the generation and storage of electrical energy should receive special attention. As the novel substances are progressively synthesized and prepared, a number of sustainable, eco-friendly energy conversion and storage mechanisms, such as in the super-capacitors, solar cells, LIB, as well as the fuel cells, would be strongly designed. As a result of their metal-like conductivity and reversible electrochemical doping/de-doping capability, conducting polymers have been regarded as encouraging substances for converting and storing energy. Molecular backbones usually consist of conjugated double bonds; moreover, the strongly conjugated polymer chains can be reversibly assigned the electrochemical features by a doping/de-doping procedure. Hence, *via* the modulation and control of the doping levels, their conductivity can be adjusted in various

ranges between 10^{-10} and 10^4 S cm^{-1}, which span the whole range from the insulators to the semi-conductors and conductors. Such conducting polymers maintain the benefits of conventional polymers like lower cost, simplified procurement, a suitable affinity for several other substances, and greater durability and flexibility. Finally, the CPs, particularly PPy PANI, and PEDOT, have adequate potential for use as the active electrode substances for electrochemical applications.

Conflicts of interest

The authors declare no competing interests.

Acknowledgements

References

1 H. Gerischer, *Principles of electrochemistry*, The CRC handbook of solid state electrochemistry, 2019.
2 W. Schmickler and E. Santos, *Interfacial electrochemistry*, Springer Science & Business Media, 2010.
3 S. Tajik, H. Beitollahi, F. Garkani Nejad, K. Zhang, Q. V. Le, H. W. Jang, S. Y. Kim and M. Shokouhimehr, *Sensors*, 2020, **20**, 3364.

4 H. Beitollahi, S. Tajik, Z. Dourandish, K. Zhang, Q. V. Le, H. W. Jang, S. Y. Kim and M. Shokouhimehr, *Sensors*, 2020, **20**, 3256.

5 B. Nikahd and M. A. Khalilzadeh, *J. Mol. Liq.*, 2016, **215**, 253.

6 Z. C. Liu, D. S. Shin, M. Shokouhimehr, K. N. Lee, B. W. Yoo, Y. K. Kim and Y. S. Lee, *Biosens. Bioelectron.*, 2007, **22**, 2891.

7 K. Zhang, K. O. Kirlikovali, R. S. Varma, Z. Jin, H. W. Jang, O. K. Farha and M. Shokouhimehr, *ACS Appl. Mater. Interfaces*, 2020, **12**, 27821.

8 Y. Shi, L. Peng, Y. Ding, Y. Zhao and G. Yu, *Chem. Soc. Rev.*, 2015, **44**, 6684.

9 S. Tajik, H. Beitollahi, S. Z. Mohammadi, M. Azimzadeh, K. Zhang, Q. V. Le, Y. Yamauchi, H. W. Jang and M. Shokouhimehr, *RSC Adv.*, 2020, **10**, 30481.

10 H. Chen, T. N. Cong, W. Yang, C. Tan, Y. Li and Y. Ding, *Prog. Nat. Sci.*, 2009, **19**, 291.

11 M. M. Farid, A. M. Khudhair, S. A. K. Razack and S. Al-Hallaj, *Energy Convers. Manage.*, 2004, **45**, 1597.

12 J. Kim, R. Kumar, A. J. Bandodkar and J. Wang, *Adv. Electron. Mater.*, 2017, **3**, 1600260.

13 H. Letheby, *J. Chem. Soc.*, 1862, **15**, 161.

14 N. Basescu, Z. X. Liu, D. Moses, A. J. Heeger, H. Naarmann and N. Theophilou, *Nature*, 1987, **327**, 403.

15 C. K. Chiang, C. R. Fincher, Y. W. Park, A. J. Heeger, H. Shirakawa, E. J. Louis and A. G. MacDiarmid, *Phys. Rev. Lett.*, 1977, **39**, 1098.

16 H. Shirakawa, E. J. Louis, A. G. MacDiarmid, C. K. Chiang and A. J. Heeger, *J. Chem. Soc., Chem. Commun.*, 1977, **16**, 578.

17 A. F. Diaz, J. I. Castillo, J. A. Logan and W. Y. Lee, *J. Electroanal. Chem. Interfacial Electrochem.*, 1981, **129**, 115.

18 Y. B. Shim and S. M. Park, *Synth. Met.*, 1989, **29**, 169.

19 Y. B. Shim, M. S. Won and S. M. Park, *J. Electrochem. Soc.*, 1990, **137**, 538.

20 D. E. Stilwell and S. M. Park, *J. Electrochem. Soc.*, 1988, **135**, 2254.

21 D. E. Stilwell and S. M. Park, *J. Electrochem. Soc.*, 1989, **136**, 427.

22 S. Tajik, H. Beitollahi, M. R. Aflatoonian, B. Mohtat, B. Aflatoonian, I. Sheikh Shoaie, M. A. Khalilzadeh, M. Ziasistani, K. Zhang, H. W. Jang and M. Shokouhimehr, *RSC Adv.*, 2020, **10**, 15171.

23 S. Tajik, H. Beitollahi, F. Garkani Nejad, M. Safaei, K. Zhang, Q. V. Le, R. S. Varma, H. W. Jang and M. Shokouhimehr, *RSC Adv.*, 2020, **10**, 21561.

24 T. Yamamoto, H. Fukumoto and T. A. Koizumi, *J. Inorg. Organomet. Polym.*, 2009, **19**, 3.

25 J. L. Bredas and G. B. Street, *Acc. Chem. Res.*, 1985, **18**, 309.

26 G. Wang, A. Morrin, M. Li, N. Liu and X. Luo, *J. Mater. Chem. B*, 2018, **6**, 4173.

27 T. O. Magu, A. U. Agobi, L. Hitler and P. M. A. Dass, *J. Chem. Rev.*, 2019, **1**, 19.

28 M. R. Aflatoonian, S. Tajik, B. Mohtat, B. Aflatoonian, I. Sheikh Shoaie, H. Beitollahi, K. Zhang, H. W. Jang and M. Shokouhimehr, *RSC Adv.*, 2020, **10**, 13021.

29 J. Simonet and J. Rault-Berthelot, *Prog. Solid State Chem.*, 1991, **21**, 1.

30 J. Huang, K. Wang and Z. Wei, *J. Mater. Chem.*, 2010, **20**, 1117.

31 G. Inzelt, *Conducting polymers: a new era in electrochemistry*, Springer Science & Business Media, 2012.

32 N. Aydemir, J. Malmström and J. Travas-Sejdic, *Phys. Chem. Chem. Phys.*, 2016, **18**, 8264.

33 D. G. Prajapati and B. Kandasubramanian, *Macromol. Chem. Phys.*, 2019, **220**, 1800561.

34 S. Tajik, Z. Dourandish, K. Zhang, H. Beitollahi, Q. V. Le, H. W. Jang and M. Shokouhimehr, *RSC Adv.*, 2020, **10**, 15406.

35 A. J. Heeger, *Handbook of conducting polymers*, ed T. A. Skotheim, New York, Marcel Dekker, 1986.

36 M. H. Naveen, N. G. Gurudatt and Y. B. Shim, *Appl. Mater. Today*, 2017, **9**, 419.

37 J. I. Kroschwitz, *Electrical and Electronic Properties of Polymers*, Wiley, New York, 1988.

38 M. Gerard, A. Chaubey and B. D. Malhotra, *Biosens. Bioelectron.*, 2002, **17**, 345.

39 T. O. Magu, A. U. Agobi, L. Hitler and P. M. Dass, *J. Chem. Rev.*, 2019, **1**, 19.

40 A. Kausar and M. Siddiq, *Polymer Science: Research Advances, Practical Applications and Educational Aspects*, 2016, p. 177.

41 A. J. Heeger, *J. Phys. Chem. B*, 2001, **36**, 8475.

42 X. X. Wang, G. F. Yu, J. Zhang, M. Yu, S. Ramakrishna and Y. Z. Long, *Prog. Mater. Sci.*, 2020, 100704.

43 P. Bocchetta, D. Frattini, M. Tagliente and F. Selleri, *Curr. Nanosci.*, 2020, **16**, 462.

44 Y. Liang and J. C. H. Goh, *Bioelectricity*, 2020, **2**, 101.

45 I. Fratoddi, I. Venditti, C. Cametti and M. V. Russo, *Sens. Actuators, B*, 2015, **220**, 534.

46 H. Nie, Y. Zhao, M. Zhang, Y. Ma, M. Baumgarten and K. Müllen, *Chem. Commun.*, 2011, **47**, 1234.

47 R. Saraswathi, M. Gerard and B. D. Malhotra, *J. Appl. Polym. Sci.*, 1999, **74**, 145.

48 F. G. Zamani, H. Moulahoum, M. Ak, D. O. Demirkol and S. Timur, *TrAC, Trends Anal. Chem.*, 2019, **118**, 264.

49 Z. Q. Feng, J. Wu, W. Cho, M. K. Leach, E. W. Franz, Y. I. Naim and D. Martin, *Polymer*, 2013, **54**, 702.

50 M. Brinkmann and P. Rannou, *Adv. Funct. Mater.*, 2007, **17**, 101.

51 A. J. Bard, J. R. Faulkner, J. Leddy and C. G. Zoski, *Electrochemical methods: fundamentals and applications*. New York, Wiley, 1980.

52 K. Zhang, K. O. Kirlikovali, Q. V. Le, Z. Jin, R. S. Varma, H. W. Jang, O. K. Farha and M. Shokouhimehr, *ACS Appl. Nano Mater.*, 2020, **3**(5), 3964.

53 S. Kempahanumakkagari, A. Deep, K. H. Kim, S. K. Kailasa and H. O. Yoon, *Biosens. Bioelectron.*, 2017, **95**, 106.

54 M. D. Rahman, P. Kumar, D. S. Park and Y. B. Shim, *Sensors*, 2008, **8**, 118.

55 H. Beitollahi, M. A. Khalilzadeh, S. Tajik, M. Safaei, K. Zhang, H. W. Jang and M. Shokouhimehr, *ACS Omega*, 2020, **5**, 2049.

56 K. Zhang, T. H. Lee, J. H. Cha, R. S. Varma, J. W. Choi, H. W. Jang and M. Shokouhimehr, *ACS Omega*, 2019, **4**, 21410.

57 S. A. Alqarni, M. A. Hussein, A. A. Ganash and A. Khan, *Bio. Nano Sci.*, 2020, **1**, 14.

58 M. Gerard, A. Chaubey and B. D. Malhotra, *Biosens. Bioelectron.*, 2002, **17**, 345.

59 S. Nambiar and J. T. Yeow, *Biosens. Bioelectron.*, 2011, **26**, 1825.

60 M. Beley and P. C. Gros, *Organometallics*, 2014, **33**, 4590.

61 R. M. Bullock, A. K. Das and A. M. Appel, *Chem.–Eur. J.*, 2017, **23**, 7626.

62 M. Ahlers, W. Müller, A. Reichert, H. Ringsdorf and J. Venzmer, *Angew. Chem., Int. Ed.*, 1990, **29**, 1269.

63 Y. Wen, X. Liao, C. Deng, G. Liu, Q. Yan, L. Li and X. Wang, *Microchim. Acta*, 2017, **184**, 935.

64 D. Dechtrirat, P. Yingyuad, P. Prajongtat, L. Chuenchom, C. Sriprachuabwong, A. Tuantranont and I. M. A. Tang, *Microchim. Acta*, 2018, **185**, 261.

65 M. Raj, P. Gupta, R. N. Goyal and Y. B. Shim, *Sens. Actuators, B*, 2017, **239**, 993.

66 M. Govindasamy, V. Mani, S. M. Chen, A. Sathiyan, J. P. Merlin and G. Boopathy, *Int. J. Electrochem. Sci.*, 2016, **11**, e10814.

67 N. A. A. Talib, F. Salam and Y. Sulaiman, *Sensors*, 2018, **18**, 4324.

68 Ş. Sağlam, A. Arman, A. Arda, B. Ustamehmetoğlu, E. Sezer and R. Apak, *Electroanal*, 2019, **32**, 964.

69 B. Deiminiat and G. H. Rounaghi, *Sens. Actuators, B*, 2018, **259**, 133.

70 H. Ghadimi, R. M. Tehrani, W. J. Basirun, N. J. Ab Aziz, N. Mohamed and S. Ab Ghani, *J. Taiwan Inst. Chem. Eng.*, 2016, **65**, 101.

71 M. Arvand, M. Farahpour and M. S. Ardaki, *Talanta*, 2018, **176**, 92.

72 M. Braik, M. M. Barsan, C. Dridi, M. B. Ali and C. M. Brett, *Sens. Actuators, B*, 2016, **236**, 574.

73 H. F. Cui, Y. F. Bai, W. W. Wu, X. He and J. H. Luong, *J. Electroanal. Chem.*, 2016, **766**, 52.

74 F. A. Harraz, A. A. Ismail, S. A. Al-Sayari, A. Al-Hajry and M. S. Al-Assiri, *Sens. Actuators, B*, 2016, **234**, 573.

75 L. Liu, H. Cui, H. An, j. Zhai and y. Pan, *Ionics*, 2017, **23**, 1517.

76 N. Wang, H. Dai, D. Wang, H. Ma and M. Lin, *Mater. Sci. Eng., C*, 2017, **76**, 139.

77 Y. Zuo, J. Xu, X. Zhu, X. Duan, L. Lu, Y. Gao and Y. Yu, *Synth. Met.*, 2016, **220**, 14.

78 K. S. Selvan and S. S. Narayanan, *J. Electroanal. Chem.*, 2018, **810**, 176.

79 I. Kazane, K. Gorgy, C. Gondran, N. Spinelli, A. Zazoua, E. Defrancq and S. Cosnier, *Anal. Chem.*, 2016, **88**, 7268.

80 I. Sadriu, S. Bouden, J. Nicolle, F. I. Podvorica, V. Bertagna, C. Berho and C. Vautrin-Ul, *Talanta*, 2020, **207**, 120222.

81 N. Kaur, H. Thakur and N. Prabhakar, *J. Electroanal. Chem.*, 2016, **775**, 121.

82 B. Xu, B. Zhang, l. Yang, F. Zhao and B. Zeng, *Electrochim. Acta*, 2017, **258**, 1413.

83 Y. Gu, J. Wang, M. Pan, S. Li, G. Fang and S. Wang, *Sens. Actuators, B*, 2019, **283**, 571.

84 O. Gursoy, S. Sen Gursoy, S. Cogal and G. Celik Cogal, *Polym. Eng. Sci.*, 2018, **58**, 839.

85 M. Bilgi and E. Ayranci, *Sens. Actuators, B*, 2016, **237**, 849.

86 Ş. U. Karabiberoğlu and Ç. C. Koçak, *Turk. J. Chem.*, 2018, **42**, 291.

87 M. Dervisevic, E. Dervisevic, H. Azak, E. Cevik, M. Şenel and H. B. Yildiz, *Sens. Actuators, B*, 2016, **225**, 181.

88 H. Mudila, P. Prasher, S. Rana, B. Khati and M. G. H. Zaidi, *Carbon Lett.*, 2018, **26**, 88.

89 A. Kausaite-Minkstimiene, L. Glumbokaite, A. Ramanaviciene, E. Dauksaite and A. Ramanavicius, *Electroanal*, 2018, **30**, 1642.

90 H. Al-Sagur, S. Komathi, M. A. Khan, A. G. Gurek and A. Hassan, *Biosens. Bioelectron.*, 2017, **92**, 638.

91 A. Shafaat, F. Faridbod and M. R. Ganjali, *New J. Chem.*, 2018, **42**, 6034.

92 V. Serafín, R. M. Torrente-Rodríguez, M. Batlle, P. G. de Frutos, S. Campuzano, P. Yáñez-Sedeño and J. M. Pingarrón, *Sens. Actuators, B*, 2017, **240**, 1251.

93 T. Kangkamano, A. Numnuam, W. Limbut, P. Kanatharana, T. Vilaivan and P. Thavarungkul, *Biosens. Bioelectron.*, 2018, **102**, 217.

94 J. Yang, Y. Liu, S. Liu, L. Li, C. Zhang and T. Liu, *Mater. Chem. Front.*, 2017, **1**, 251.

95 J. G. Ibanez, M. E. Rincón, S. Gutierrez-Granados, M. H. Chahma, O. A. Jaramillo-Quintero and B. A. Frontana-Uribe, *Chem. Rev.*, 2018, **118**, 4731.

96 P. Sivaraman, A. P. Thakur and K. Shashidhara, *Synth. Met.*, 2020, **259**, 116255.

97 Y. Ge, R. Jalili, C. Wang, T. Zheng, Y. Chao and G. G. A. Wallace, *Electrochim. Acta*, 2017, **235**, 348.

98 Y. Li, J. Niu, T. Xue, X. Duan, Q. Tian, Y. Wen and Z. Li, *J. Electrochem. Soc.*, 2020, **167**, 047512.

99 Z. Wang, P. Tammela, J. Huo, P. Zhang, M. Strømme and L. Nyholm, *J. Mater. Chem. A*, 2016, **4**, 1714.

100 Y. He, X. Han, Y. Du, B. Song, P. Xu and B. Zhang, *ACS Appl. Mater. Interfaces.*, 2016, **8**, 3601.

101 R. K. Jena, C. Y. Yue, M. M. Sk and K. A. Ghosh, *Carbon*, 2017, **115**, 175.

102 D. Zhu, K. Cheng, Y. Wang, D. Sun, L. Gan, T. Chen and M. Liu, *Electrochim. Acta*, 2017, **224**, 17.

103 S. Ji, J. Yang, J. Cao, X. Zhao, M. A. Mohammed, P. He and I. A. A. Kinloch, *ACS Appl. Mater. Interfaces*, 2020, **12**, 13386.

104 J. M. D'Arcy, H. D. Tran, V. C. Tung, A. K. Tucker-Schwartz, R. P. Wong, Y. Yang and R. B. Kaner, *Proc. Natl. Acad. Sci.*, 2010, **107**, 19673.

105 C. Houarner-Rassin, E. Blart, P. Buvat and F. Odobel, *Photochem. Photobiol. Sci.*, 2008, **7**, 789.

106 Y. S. Gal, S. H. Jin, S. Y. Shim and K. T. Lim, *Mol. Cryst. Liq. Cryst.*, 2017, **654**(1), 83.

107 S. A. Gopalan, A. I. Gopalan, A. Vinu, K. P. Lee and S. W. A. Kang, *Sol. Energy Mater. Sol. Cells*, 2018, **174**, 112.

108 S. Alem, N. Graddage, J. Lu, T. Kololuoma, R. Movileanu and Y. Tao, *Org. Electron.*, 2018, **52**, 146.

109 E. H. Jung, N. J. Jeon, E. Y. Park, C. S. Moon, T. J. Shin, T. Y. Yang and J. Seo, *Nature*, 2019, **567**, 511.

110 N. Sangiorgi, A. Sangiorgi, F. Tarterini and A. Sanson, *Electrochim. Acta*, 2019, **305**, 322.

111 A. V. Murugan, T. Muraliganth and A. Manthiram, *Electrochem. Commun.*, 2008, **10**, 903.

112 M. Tian and P. Wu, *ACS Appl. Energy Mater.*, 2019, **2**, 5066.

113 W. Zeng, L. Wang, X. Peng, T. Liu, Y. Jiang, F. Qin and Y. Zhou, *Adv. Energy Mater.*, 2018, **8**, 1702314.

114 Q. T. Wang, R. R. Li, X. Z. Zhou, J. Li and Z. Q. Lei, *J. Solid State Electrochem.*, 2016, **20**, 1331.

115 K. Hua, X. Li, D. Fang, J. Yi, X. Wu, Z. Luo and S. Wang, *Mater. Sci. Eng., B*, 2018, **238**, 26.

116 M. S. Wang, Z. Q. Wang, Z. Chen, Z. L. Yang, Z. L. Tang, H. Y. Luo and W. Xu, *Chem. Eng. J.*, 2018, **334**, 162.

117 H. Li, S. Yang, Y. Zhao, T. Tan, X. Wang and Z. Bakenov, *J. Nanomater.*, 2019, 4702849.

118 L. A. Fard, R. Ojani, J. B. Raoof, E. N. Zare and M. M. Lakouraj, *Appl. Surf. Sci.*, 2017, **401**, 40.

119 R. Dillon, S. Srinivasan, A. S. Arico and V. Antonucci, *J. Power Sources*, 2004, **127**, 112.

120 C. H. Choi, K. Chung, T. T. Nguyen and D. H. Kim, *ACS Energy Lett.*, 2018, **3**, 1415.

121 S. Tajik, H. Beitollahi, M. R. Aflatoonian, B. Aflatoonian, I. Sheikh Shoaie, M. A. Khalilzadeh, K. Zhang, Q. V. Le, H. W. Jang and M. Shokouhimehr, *Microchem. J.*, 2020, **157**, 104890.

122 Z. Yang, Z. Yao, G. Li, G. Fang, H. Nie, Z. Liu and S. Huang, *ACS Nano*, 2012, **6**, 205.

123 Z. Yang, H. Nie, X. Chen and S. Huang, *J. Power Sources*, 2013, **236**, 238.

124 J. Peron, Z. Shi and S. Holdcroft, *Energy Environ. Sci.*, 2011, **4**, 1575.

125 V. G. Khomenko, V. Z. Barsukov and A. S. Katashinskii, *Electrochim. Acta*, 2005, **50**, 1675.

126 M. G. A. El-Moghny, H. H. Alalawy, A. M. Mohammad, A. A. Mazhar, M. S. El-Deab and B. E. El-Anadouli, *Int. J. Hydrogen Energy*, 2017, **42**, 11166.

127 E. Miglbauer, P. J. Wójcik and E. D. Głowacki, *Chem. Commun.*, 2018, **54**, 11873.

128 A. El Attar, L. Oularbi, S. Chemchoub and M. El Rhazi, *Int. J. Hydrogen Energy*, 2020, **45**, 8887.

129 K. Zhang, J. H. Cha, S. Y. Jeon, K. O. Kirlikovali, M. Ostadhassan, V. Rasouli, O. K. Farha, H. W. Jang, R. S. Varma and M. Shokouhimehr, *Mol. Catal.*, 2020, **492**, 110967.

130 K. Zhang, T. H. Lee, H. Noh, O. K. Farha, H. W. Jang, J. W. Choi and M. Shokouhimehr, *Cryst. Growth Des.*, 2019, **19**, 7385.

131 K. Zhang, K. O. Kirlikovali, J. M. Suh, J. W. Choi, H. W. Jang, R. S. Varma, O. K. Farha and M. Shokouhimehr, *ACS Appl. Energy Mater.*, 2020, **3**, 6019.